

MELT FRACTURE OF POLYSTYRENE

MELT FRACTURE OF POLYSTYRENE

by

STATHIS LIDORIKIS, DIPL. ENG.

A Thesis

Submitted to the Faculty of Graduate Studies
in Partial Fulfilment of the Requirements
for the Degree
Master of Engineering

McMaster University

September 1970

MASTER OF ENGINEERING (1970)
(Chemical Engineering)

McMASTER UNIVERSITY
Hamilton, Ontario

TITLE: Melt Fracture of Polystyrene

AUTHOR: Stathis Lidorikis, Dipl. Eng. (Technical University
of Greece)

SUPERVISOR: Dr. J. Vlachopoulos

NUMBER OF PAGES: viii, 112

ABSTRACT

A high-pressure nitrogen-driven viscometer has been used to study the melt fracture of polystyrene. The polystyrene samples used differed in molecular weight and molecular weight distribution. The weight average molecular weight (\bar{M}_w) ranged from 97,200 to 1.8×10^6 and the distribution breadth (\bar{M}_w/\bar{M}_n) from 1.06 to 9.21. Results obtained indicate that the critical shear stress varies linearly with $1/\bar{M}_w$, increases slightly with temperature and is independent of the polydispersity of polymers. This type of behaviour is satisfactorily explained in terms of Graessley's entanglement theory.

ACKNOWLEDGEMENTS

The author wishes to express his gratitude to his research advisor, Dr. John Vlachopoulos for his constant guidance, advice in data interpretation, materials preparation, and most of all, for his encouragement.

Also the author would like to express his thanks to Mr. M. Alaw for his assistance in this investigation.

Gratitude is also due to the Department of Chemical Engineering, McMaster University, for its financial support to the author.

Last but not least, the author is grateful to his wife, Cristin, for her patience, understanding and sacrifices during the period of preparation of this work.

TABLE OF CONTENTS

	Page
1. INTRODUCTION	1
1.1 General	1
1.2 Nature of Polymer Molecules	2
1.3 The Rheology of Polymers	4
1.4 Rheological Classification	6
1.5 Objectives of Thesis	9
2. GENERAL DESCRIPTION OF FLOW DEFECTS	10
2.1 General	10
2.2 Swelling	10
2.3 Mattness	10
2.4 Sharkskin	11
2.4.1 Influence of extrusion variables	11
2.4.2 Effect of molecular structure	12
2.5 Melt Fracture	12
3. MELT FRACTURE. SELECTED LITERATURE SURVEY	14
3.1 Mechanism	14
3.1.1 Turbulence	14
3.1.2 Outlet phenomena	15
3.1.3 Viscous heating	16
3.1.4 Fracture hypothesis	16
3.1.5 Stick-slip mechanism	18
3.1.6 Elastic energy hypothesis	19
3.2 Influence of Extrusion Variables	22

	Page
3.3 Effect of Molecular Structure	24
3.3.1 Molecular weight	24
3.3.2 Molecular weight distribution	25
4. CAPILLARY FLOW	26
4.1 Theory	26
4.2 Errors in Capillary Flow	33
4.2.1 Slip at the wall	33
4.2.2 End effects	35
4.2.3 Heat effects	40
4.2.4 Laminar flow	49
4.2.5 Expansion of the fluid	49
4.3 Normal Stress Effects	50
5. EXPERIMENTAL WORK	55
5.1 Apparatus	55
5.2 Materials	59
5.3 Treatment of Data	61
6. RESULTS AND DISCUSSION	63
7. ANALYSIS	76
8. CONCLUSIONS	85
9. NOMENCLATURE	86
REFERENCES	90
APPENDICES	95
APPENDIX I	96
APPENDIX II	109
APPENDIX III	111

LIST OF TABLES

	Page
Table I Diameters and Length/Diameter Ratios of Capillary Tubes	57
Table II Polymer Samples Used	60
Table III Critical Conditions of Polystyrene	69

LIST OF FIGURES

	Page
Figure 1. Typical Polymer Molecule	2
Figure 2. Specimens of Polystyrene Extruded at Successively higher shear rates at 170°C	13
Figure 3. Schematic Illustration of the Flow in a Capillary Tube	27
Figure 4. Regions Associated with Flow Through Tubes	37
Figure 5. Correction of the Tube Length by the Addition of Length ND in order to Calculate the Pressure Gradient	38
Figure 6. Dimensionless Wall Temperature Rise Down the Length of a Capillary Due to Viscous Heating	46
Figure 7. Nomograph for Estimation of Temperature Rise Due to Viscous Dissipation	48
Figure 8. Manual Rheometer	56
Figure 9. Flow Curves for Polystyrene	64
Figure 10. Curves of Pressure versus L/D	65
Figure 11. Apparent Shear Rate versus Corrected Shear Stress	66
Figure 12. Corrected Flow Curve for Polystyrene	67
Figure 13. Apparent Viscosity versus Shear Rate	68
Figure 14. Critical Shear Stress Dependence on Temperature	71
Figure 15. Critical Shear Stress versus $1/\bar{M}_w$	72
Figure 16. Dependence of $\tau_{cr} \times \bar{M}_w$ on \bar{M}_w	73
Figure 17. Critical Shear Stress versus $1/\bar{M}_w$	75
Figure 18. Critical Shear Stress from Entanglement Theory versus $1/\bar{M}_w$	84

1. INTRODUCTION

1.1 General

Engineering interest and involvement in non-Newtonian fluid technology has developed largely within the past fifteen years. While industrial experience with non-Newtonian materials has a far longer history, the systematic study and characterization of mass, heat and momentum transfer processes in these systems is of recent origin. Prior to this time the approach and techniques available for the study and interpretation of such processes were principally those of Newtonian fluid mechanics and design and scale-up criteria required exhaustive experimental studies.

However, for many processes in non-Newtonian systems, design and scale-up criteria are now based upon the rheological characteristics of the fluid media. Once such characterization is made, the results are readily applied with a minimum requirement for further experimental studies.

The continuing growth and competition in the plastics, fiber, and elastomer industries have made clear the necessity of a deeper understanding of the processing behaviour of polymers and of obtaining quantitative methods for prediction of the rheological properties of these materials as they flow

through dies and spinnerets, between calender rolls, and screw and barrel of extruders.

1.2 Nature of Polymer Molecules

The word polymer is generally used to describe a large molecule composed of many small primary molecules chemically bound together. The primary molecules are usually referred to as "monomer units" and the number Z of monomer units in the polymer is called the "degree of polymerization". In spite of the fact that even dimers (i.e., $Z=2$) are polymer molecules, the "degree of polymerization" may reach ten thousand before the reaction terminates, and so molecular weights may be of the order of millions. A typical polymer molecule will therefore consist of a long chainlike structure such as that shown in Figure 1. This chain will in general be of appreciable length, so that it can ordinarily be considered even more flexible than the picture would indicate. Moreover, Brownian motion will cause the chain to writhe and squirm, and it will change its configuration continuously under the action of thermal motion.

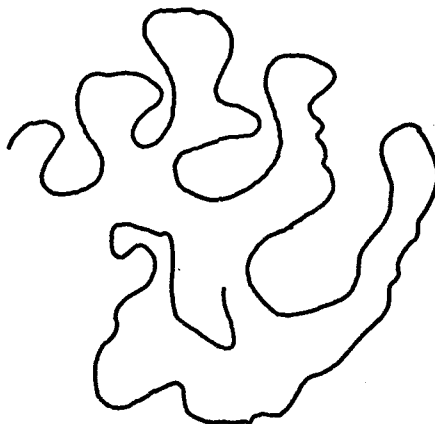


FIG. 1. TYPICAL POLYMER MOLECULE .

Although the number Z of primary molecules composing the polymer molecule is quite definite for any given molecule, the methods of preparation of these macromolecules usually preclude the possibility of a sample in which all the polymer molecules contain the same number of primary molecules. Thus, most commercial polymers are mixtures of chains of various molecular weights. It is generally acceptable that the distribution of molecular weights in a polymer sample has a marked influence upon the physical behaviour of the material; hence, it is important to have ways of characterizing the distribution. One may define a molecular weight distribution function and various molecular weight "averages" for a polymer sample. (Although molecular weight is a discrete variable, a continuous distribution function can be used.) Suppose, for example, that one denotes the number fraction of chains of molecular weight in the range M to $M + dM$ by $f(M)$. Then the "number average molecular weight" \bar{M}_n is defined by

$$\bar{M}_n = \int_0^{\infty} M f(M) dM \quad (1-1)$$

and the "weight average molecular weight" \bar{M}_w is defined by

$$\bar{M}_w = \int_0^{\infty} M^2 f(M) dM / \int_0^{\infty} M f(M) dM \quad (1-2)$$

Other averages may be defined, and the relationships among the various averages depend upon the particular molecular weight distribution.

It should be pointed out, however, that one reason for defining different molecular weight averages lies in the fact that certain experimental techniques are sensitive to different moments of the molecular weight distribution, that is, to different average molecular weights. For polydisperse polymers the weight average \bar{M}_w is found to be larger than the number average \bar{M}_n . The ratio \bar{M}_w/\bar{M}_n is a measure of the breadth of the molecular weight distribution.

1.3 The Rheology of Polymers

Conventional measurements for the study of the properties of polymers were of two types.

- a) Measurements of "physical" properties, carried out on solid specimens (e.g. tensile tests).
- b) Measurements of "molecular" properties, carried out on dilute solutions (e.g. measurement of intrinsic viscosity, osmotic molecular weight).

In the last few years the development of suitable instruments has made possible the observation of the rheological characteristics of molten polymers. It has thus become possible to establish correlations between these characteristics and both the molecular properties of molten polymers and the physical behaviour of solid polymers.

The study of polymeric fluids is but a small part of the broader field called rheology. It has come to include almost every aspect of the study of the deformation of matter under the

influence of imposed stress; it is the study of the internal response of materials to forces.

Several broad, qualitative categories of response can be described. If a small stress is suddenly exerted on a solid a deformation will begin to occur. The material will continue to deform until molecular (internal) stresses are established which just balance the external stresses (equilibrium deformation). Most solids exhibit some degree of elastic response, in which there is complete recovery of deformation upon removal of the deforming stresses. The simplest such body is the Hookean elastic solid, for which the deformation is directly proportional to the applied stress.

Not all materials reach an equilibrium deformation. A fluid response is one in which there is no resistance to deformation. In such a fluid, if an external stress is exerted, deformation occurs, and continues to occur indefinitely until the stress is removed. But internal frictional forces retard the rate of deformation, and an equilibrium can be established in which the rate of deformation is constant and related to the properties of the fluid. The simplest such fluid is the Newtonian fluid, in which the rate of deformation is directly proportional to the applied stress. However, many fluids exhibit a non-linear response to stress and are called, collectively, non-Newtonian fluids. Most synthetic polymer solutions and melts exhibit some degree of non-Newtonian behaviour.

1.4 Rheological Classification

Gases and liquids of low molecular weight are "Newtonian", meaning that their viscosity is independent from the flow conditions and dependent solely upon temperature and composition. Hence, only one viscosity value is sufficient in order to describe their behaviour in the same way that one value of a solid's elasticity module describes its behaviour toward a certain kind of deformation. The viscosity of molten polymers though can easily change by a factor of 10^4 as a function of the flow conditions and it may be necessary to measure it in a larger shear range. Thus, the rheological properties of a polymer will not be completely defined, at each temperature, by a single viscosity value, but by a flow diagram, giving the values of viscosity as a function of shear rate, or other parameters of flow.

In the following, the more common variables one encounters in rheology will be described: the viscosity of a fluid undergoing a laminar motion in the so-called "steady flow" is given by

$$\eta = \frac{\tau}{\dot{\gamma}} \quad (1-3)$$

and is called the "apparent viscosity" in the case of non-Newtonian fluids. The "shear stress" τ is the stress originating the viscous motion and it is defined as the ratio of the force F , tangentially applied to a flowing surface S , and the surface S :

$$\tau = F/S \quad (1-4)$$

The shear stress τ is not a pressure although its dimensions correspond to a pressure. The neighbouring elements of any viscous fluid have different velocities V_z . The shear rate $\dot{\gamma}$ is defined as the gradient of the velocity of the flowing liquid, and it is given by:

$$\dot{\gamma} = \frac{dV_z}{dr} \quad (1-5)$$

where r is perpendicular to the flow direction.

The viscosity η is the coefficient of internal friction measuring the resistance of a given material to motion. The relation between η and $\dot{\gamma}$:

$$\eta = f(\dot{\gamma}) \quad \text{or} \quad \tau = f(\dot{\gamma}) \quad (1-6)$$

defines the rheological behaviour of the liquids. The flow curves are diagrams of shear stress as a function of the velocity gradient $\dot{\gamma}$ or

$$\tau = f(\dot{\gamma})$$

The simplest type of flow curve is obtained when τ is a linear function of $\dot{\gamma}$. The ratio $\eta = \tau/\dot{\gamma}$ is then constant and only one viscosity value describes the rheological behaviour. The liquid is a "Newtonian" one. Non-Newtonian fluids such as oils, plastisols, molten polymers, do not have a constant viscosity and the relation $\tau = f(\dot{\gamma})$ may be of different kinds, and even hard to describe mathematically. However, it can still be used to describe the rheological character of the different systems. In fact, the relation

$$\tau = k_0(\dot{\gamma})^n \quad (1-7)$$

where n and k_0 are constants (it is called the "power law") describes quite well the flow curves of many materials for large intervals of $\dot{\gamma}$ and it can be useful also for classifying the fluids:

For $n < 1$ a fluid is called "pseudo plastic". The slope of the flow curves becomes smaller with increasing $\dot{\gamma}$ and the viscosity $\eta = \tau/\dot{\gamma}$ diminishes with an increase of the shear rate (or τ which is the equivalent). Almost every molten polymer behaves as a pseudoplast within a given shear rate range, while out of this range they can behave as Newtonian fluids.

For $n > 1$ the fluids are called "dilatant" ones. In such systems the viscosity increases with increasing shear rate $\dot{\gamma}$ or the shear stress τ . Many heterogeneous systems, suspensions and plastisols are "dilatant".

The above classification applies only to "viscous" fluid systems, in which the energy causing deformation is dissipated as heat. For "elastic" systems, energy is stored as potential energy. In this case, the deformation is reversible. Molten polymers behave as "viscoelastic" systems, since they can absorb energy in both ways at the same time. The fraction of energy being elastically stored during the flow is a function of the system under examination of temperature, of the deformation velocity and the employed instrument. The elastic defor-

mation experienced by the polymers under flow might or might not follow Hooke's law.

1.5 Objectives of Thesis

In the flow of amorphous or molten polymers through capillaries, a rather striking phenomenon occurs called melt fracture (1,2, 3). This phenomenon manifests itself as a gross distortion of the extrudate which can take various forms such as, for example, a regular helix of wave-length comparable with the diameter, a zig-zag distortion, irregular convolutions or even complete fragmentation.

The purpose of this investigation is to explain the nature of this phenomenon and how it is related to the molecular structure of the polymer.

2. GENERAL DESCRIPTION OF FLOW DEFECTS

2.1 General

During the extrusion of molten polymers at high stresses it is frequently found that the surface or shape of the extrudate is impaired by the presence of flow defects. The various flow defects shown by different polymers are of great importance in polymer processing. The most important of these defects are: swelling, mattness, sharkskin, melt fracture.

2.2 Swelling

When certain non-Newtonian fluids are ejected from an orifice or tube, the resulting jet is commonly observed to expand to a diameter much larger than its initial ejection diameter. This effect is sometimes called the "Barus phenomenon" and is usually referred to industrially as "die swell" or "extrudate swelling". This effect has variously been attributed to polymer memory of conditions before the die, to shear recovery (4), to normal forces, and to the change from a paraboloidal distribution of velocities within the die to a flat velocity profile in the solid extrudate (5).

2.3 Mattness

This phenomenon consists of a loss of surface gloss. Mattness does not initiate at a critical stress, and was not examined in the present investigation.

2.4 Sharkskin

This defect gives finely spaced, sharp, regular, circumferential ridges in the extrudate. It has not been investigated by so many workers as has melt fracture. This is probably due to the fact that it is not such a catastrophic phenomenon and can often be tolerated to a certain degree.

There is general agreement amongst workers in this field that sharkskin is formed either in the die land or at the exit. Howells and Benbow (6) propose that the principal cause of this defect is the cyclic build-up and release of surface tensile forces in the extrudate at the die exit. It is also suggested by these authors and others (7, 8) that a type of stick-slip mechanism is involved, and it seems probable that both these mechanisms are closely related to each other and to the other view of Kendall (8) that sharkskin is due to differential recovery between the skin and core.

2.4.1 Influence of extrusion variables

There is general agreement among the workers who have investigated sharkskin that, for a particular polymer, sharkskin occurs at a fixed linear velocity rather than at a critical shear rate (6, 7, 9). This is well illustrated by Clegg (7) who showed that the onset of sharkskin is independent of die diameter but considerably delayed by increasing temperature. It is also generally agreed by the same workers that die entry angle does not influence the onset of sharkskin.

2.4.2 Effect of molecular structure

The information available on the effect of molecular structure on sharkskin is incomplete. However, it is generally acceptable that sharkskin is not very dependent upon molecular weight but is much more severe for narrow than for wide molecular weight distribution (MWD) materials (10).

The noticeable characteristic of these defects (mattness, sharkskin) is that they leave the rest of the flow effectively unaltered.

2.5 Melt Fracture

The flow of molten polymers through dies can be disrupted by the onset of a flow instability called melt fracture, which exhibits itself as a gross distortion of the extrudate.

Although considerable research effort has been expended on melt fracture, the problem has not been eliminated from plastics processing. There is no general agreement among the investigators in the explanation of this phenomenon regarding its mechanism and the effects of extrusion variables and molecular structure on it.

Figure 2 is an illustration of the development of this type of irregularity with increase in shear rate for polystyrene of $\bar{M}_w = 355,000$ at 170°C . For $4Q/\pi r_o^3 = 27 \text{ sec}^{-1}$ the extrudate is smooth. For $4Q/\pi r_o^3 = 83 \text{ sec}^{-1}$ the extrudate is irregular (incipience of melt fracture). For $4Q/\pi r_o^3 = 240 \text{ sec}^{-1}$ there is a pronounced distortion of the extrudate.

$$\bar{M}_w = 355,000$$

$$\frac{\bar{M}_w}{\bar{M}_n} = 2.92$$

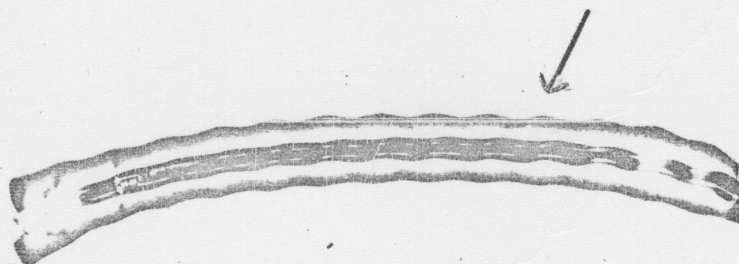
Temperature 170°C

$$\frac{4Q}{\eta r_0^3} \quad \tau_{ap} \times 10^{-5}$$

sec⁻¹ dynes/cm²



3.8 10.3



19.0 18.2



38.1 29.2

Fig. 2. Specimens of polystyrene extruded at successively higher shear rates at 170°C. The arrow indicates the first appearance of waviness.

3. MELT FRACTURE. SELECTED LITERATURE SURVEY

3.1 Mechanism

The gross extrudate distortion described as "melt fracture", "elastic turbulence", "waviness", "knobbliness" or "bambooning" is recognized as a departure from smooth flow which arises because polymer melts are elastic as well as viscous. This is why the phrase "elastic turbulence" is used, although it is clear that the phenomenon is not turbulent in the classical Reynolds sense.

A number of mechanisms have been proposed for the phenomenon of "melt fracture", the most important of which are (ii): Reynolds turbulence, outlet phenomena, "viscous" heating, Fracture hypothesis, stick-slip mechanism, elastic energy hypothesis.

3.1.1 Turbulence

The first theory for melt fracture, proposed by Nason (1) and supported later by Westover and Maxwell (12), was on the basis of conventional turbulence in the classical Reynolds sense (i.e., when the Reynolds number, the relationship between inertia and viscous forces, exceeded a given value). The usual criterion for onset of turbulence involves a critical value of the Reynolds number. The Reynolds number is

$$Re = V_m \rho r_o / \eta = (Q / r_o \eta) (\rho / n) \quad (3-1)$$

where V_m is the mean velocity of flow, Q the volumetric flow rate, r_0 the capillary radius, η the viscosity, and ρ the density. As it was pointed out by Tordella (13), if Reynolds turbulence does occur, then the critical flow rate will vary as the first power of the capillary radius and directly with viscosity. In contrast, Tordella found that the critical flow rate, in which wavy-type distortion occurs, varies nearly inversely with the third power of the radius of the capillary.

On the basis of extensive experimental data (14) it has been shown that turbulence in non-Newtonian systems does not occur until Reynolds numbers of the order 2100 are reached, as in the case of Newtonian behaviour. The maximum value of the generalized Reynolds number at the inception of irregularities in the work of Westover and Maxwell is 1.6×10^{-4} . Thus, it is safe to say that melt fracture does not involve Reynolds turbulence (that is, energy is not dissipated into inertial eddies).

3.1.2 Outlet phenomena

A second theory (2) was that the distortion was due to the differential orientation between the extrudate skin and core causing an unstable system. They proposed that progressive increases in molecular orientation must accompany increase in shearing rate as one moves radially from the center line of the tube toward the wall. The re-randomizing of molecular orientation as shearing stresses (hence shearing rates) are removed

upon emergence of the fluid from the tube would cause a greater contraction at the surface of the filament than at the center line. This buckling of the emerging stream was presumed to occur when a critical differential elastic strain between the core and the outer surface of the stream was exceeded. This theory is now more in favour in connection with sharkskin than with melt fracture.

3.1.3 Viscous heating

This mechanism is based on temperature dependence of viscosity (15, 16, 17) and notions of a thermal catastrophe. It has been postulated that at some stress the heat generation might reduce the viscosity at or near the capillary surface sufficiently to cause instabilities of the type under discussion. But it has been shown (18) that the magnitude of the temperature rise is no more than 2°C in polyethylene. So viscous heating effects seem unimportant.

3.1.4 Fracture hypothesis

According to this hypothesis melt fracture is caused because of disruption of molecular network at sufficient stresses (19, 20). Fracture occurs due to a failure of the melt to sustain the high elastic tensile stresses which arise in the die-entry region. It is this local melt network breakdown that causes the observable back-flow or recoil near the die entry.

The idea of melt fracture near the die entry is also supported by Tordella (3, 21, 22, 23). The noise which occurred in association with the distortion was considered by Tordella to be indicative of a type of fracture. Papers by Metzner et al. (24), Beynon and Clyde (25), Clegg (7), Bagley and Birks (26), Mills et al. (27), and Schulken and Boy (28) give general support to the idea that melt fracture is caused by a fracture or tearing of the melt in the die entry region.

Reiner (29) proposed that rupture would occur in viscoelastic liquids when the stress reached a definite limit equivalent to the strength of the material. This hypothesis was not supported by Tordella (11) who says that failure of this type would involve, primarily, short-range dispersion forces. Were this the case, the failure stress would be expected to decrease with increasing temperature; dispersion forces decrease with increasing temperature due to increasing free volume. Similarly, failure stress should increase with molecular weight. Free volume decreases as the volume fraction of covalent bonds increases with molecular weight. The effect is a smaller average interchain distance and increased dispersion forces.

Since the effects of temperature and molecular weight are opposite to those predicted by dispersion force considerations, the "melt fracture" does not seem to be of a type similar to that proposed by Reiner.

3.1.5 Stick-slip mechanism

Howells and Benbow in their paper (6), whilst supporting a network breakdown in the region of the die entry, also allowed that slip between polymer and die wall may be a contributory factor.

In a paper published in 1963, Benbow and Lamb (30) report various experiments, including motion pictures of markers flowing in transparent dies, which led them to conclude that the distortion phenomenon known as elastic turbulence or melt fracture originated in a stick-slip action at the die surface. Because of the accelerative effects at the die entry this would be the favoured initiation point, but initiation could also occur in the die rather than at the entry. This slip theory had some support in the work of Kennoway (31) who obtained results for the adhesion of molten polyethylene, polymethylmethacrylate and unplasticized PVC.

The mechanism of stick-slip at the die wall has been investigated very carefully by Galt and Maxwell (32, 33) who employed carborundum particles in low-density polyethylene and showed that only 25 per cent of particles near the wall had zero velocities, that is, considerable slip occurred. Lypton and Regester (18) obtained results for high-density polyethylene which confirmed slipping at the wall and also found that in the vicinity of turbulence, where there was a discontinuity in the flow curve, the slip velocity increased very rapidly. Westover (34) concludes that for high-density polyethylene, slip is more

dependent upon a critical shear stress within the polymer or at the die wall than upon a frictional effect.

To summarize the findings on stick-slip, therefore, the latest belief is that above a certain critical stress, intermittent slipping occurs at the die wall to relieve momentarily the recoverable elastic strain to which the material has been subjected in its passage through the die and which, at lower stresses, manifests itself as uniform die swell. The releasing of the stored-up elastic energy, possibly assisted by a local temperature rise during slip, causes the melt to adhere again to the die surface. The extrudate thus emerges in a distorted form, showing intermittent rather than uniform swell, the degree of distortion depending on the shear stress. It seems reasonable to expect the greatest tendency for slip in the die entry region where the rate of change of stress and shear rate are highest. If this is the case, then the influence of die entry angle on turbulence is more easy to understand than if the first slip occurred in the die land.

3.1.6 Elastic energy hypothesis

This hypothesis merely points to elastic energy contained within the flowing melt as the likely source of instability (18, 35).

Some authors consider that the Weissenberg number, representing the balance between difference of normal and shear stresses and itself a function of the local shear rate in

steady flow, should be a useful defining parameter (35), and according to White (35) this number becomes equal to the recoverable elastic strain.

Other authors think that it is acceleration effects in the entry region that are critical and so are led to consider the Deborah number (36) which compares the characteristic of the fluid with the characteristic time of the motion. Still others seek a more direct measure of elastic effects and use the recoverable elastic strain (also a function of rate of shear) as the relevant parameter. This again is to be thought of as a directly measurable dimensionless quantity, but it can be defined in various ways, depending on the type of deformation from which recovery is measured. In the particular definitions considered by White (35) the Weissenberg number becomes equal to the recoverable elastic strain.

The possibility that unstable flow occurs when a critical elastic strain is exceeded appears worthy of consideration. That characteristic which distinguishes molten polymers from other liquids is their ability to deform elastically. Distortion of the coiled molecules from their equilibrium configuration occurs in shear and constitutes the elastic strain. Substantial elastic strain is imposed at shear rates at which "melt fracture" occurs.

Spencer and Dillon in their early work (2) found that the onset inlet melt fracture was characterized by a critical average elastic strain of about 3 units. The strain was

assessed from the degree of swelling of the emerging polymer stream. Bagley (37), using a correlation of Philippoff and Gaskins (38) between the inlet correction and elastic strain, found a critical value of about 15 strain units for branched polyethylene and 6 for linear polyethylene, 7 for polystyrene and polymethylmethacrylate. Tordella (39) and Menefee (40) found a critical value of 5 units for a variety of polymers, including both branched and linear polyethylene.

According to this mechanism, fracture involves the time-dependent character of the viscoelastic polymers. At short times deformation of molten polymers is not merely a viscous process. Substantial elastic strain is imposed and failure is consequent upon inability of the structure to deform further elastically.

Support for the critical strain, fracture hypothesis, is found in the experiments of Philippoff and Gaskins (38) with solutions of polyisobutylene. Recoverable, elastic shear strain of these solutions increased linearly with stress up to 10 or 12 units: Hooke's law in shear applied in this range. Beyond this limiting strain, shear strain increased sharply with stress to a level of about 600 units. Apparently, polymer molecules in solution disentangle and uncoil at strains above a critical strain. In bulk, rupture or fracture appears to result instead.

3.2 Influence of Extrusion Variables

The workers cited above generally agree that streamlining the die entry reduces the tendency for turbulence. Tordella (3) reported that there was a 12-fold increase in critical rate in changing from a flat entry to one of 20° included angle. Other people have not found such a large improvement, and in particular Metzner et al. (24), and Metzger et al. (41), have reported that in the angle range 180° - 40° there is virtually no improvement. However, in the former work (24), results between 40° and 20° showed a marked increase in critical rate.

Hammond (42) and Ferrari (43) have carried out very detailed experiments to optimize die design for wire coating. Hammond worked with low-density polyethylene and determined critical rates for various entry angles with different flow grades. He concluded that for best results a multiple angle die, such as $20/8/3^\circ$, with a land length of about 10:1 should be used. Ferrari carried out similar work with high-density polyethylene, polypropylene, foamed polypropylene and PVC. He found that polypropylene was very sensitive to entry angle but that PVC was relatively unaffected by changes in angle although very sensitive to changes in land length. Foamed polypropylene showed a 10 to 20 per cent higher critical rate than normal polypropylene. The best die design was concluded to be one with an initial entry of 60° , changing in a conical manner to the final parallel section. This die gave 15 times the critical rate of a single taper die of the same length.

Tordella (3) reports that apparent critical stress values were higher for smaller length/diameter (L/D) ratios; later work does not mention the effect on stress but there is general agreement (24, 41) that the critical shear rate for melt fracture is increased by increasing L/D and also that the severity of turbulence is reduced for longer dies (8, 9, 39). Metzner et al. (24) report an interesting experiment in which they extruded from an "infinite" tube with no entry region, previously filled at low pressure and allowed to relax for about 10 hours. Under normal extrusion conditions turbulence was obtained at 135 sec^{-1} , but with the entry-free experiment the extrusion at this shear rate was completely smooth. From this it was concluded that the entry provided the site for melt fracture.

In view of the dependence of apparent critical stress on ratio L/D, it might appear desirable to do all experimental work in long capillaries wherein inlet losses are negligible. There are valid reasons for working in short capillaries. First, the degree of distortion of the emerging stream decreases with increasing L/D. Consequently, critical rate may be difficult to detect using long capillaries with the result that use of short capillaries can be more convenient. Secondly, short capillaries are technologically important, and knowledge of the variation of critical stress with L/D may be desired.

The influence of die diameter has not been evaluated thoroughly but Westover and Maxwell (12) and Tordella (39)

report that larger diameters are more prone to turbulence.

Several workers have examined the influence of die finish and material of die construction on melt fracture. It is agreed (30, 44) that finish has no effect, although small but apparently significant differences in critical stress were found for capillaries of different materials of construction (30). Branched polyethylene was found to have a critical stress of about 1.5×10^6 dyn/cm² in brass, nylon, and copper capillaries, 1.3×10^6 dyn/cm² in capillaries of nickel, silver, and steel, and 1.0×10^6 dyn/cm² in capillaries of phosphor bronze, and "silver steel".

Studies by Tordella (3, 22) and Spencer and Dillon (2) on fracture of a variety of polymers showed that the critical shearing stress corresponding to incipient occurrence of irregularities was temperature-independent for polyethylene from 130° to 240°, for polystyrene from 210° to 260°, and for methacrylate from 140° to 220°C. For PVC the reverse relationship has been found (45). There is, however, general agreement that increasing temperature gives a higher critical extrusion rate before "turbulence".

3.3 Effect of Molecular Structure

3.3.1 Molecular weight

The idea that melt fracture is caused by a failure of the elastic network suggests that it should occur more readily the higher the molecular weight, since longer molecules form a

more entangled network which, because of the restrictions to flow, caused by entanglements points, is broken down at a lower rate of shear than would be the case for a low molecular weight. Most workers (2, 27, 37) have found that as molecular weight decreases, critical stress increases; in fact, the product of molecular weight and critical stress is approximately constant (2, 37). For PVC, however, Sieglaff (45) does not support this conclusion. Also Barnett's (46) data on polypropylene show that the product of molecular weight and critical shear stress is not a constant but the critical shear stress is constant. So far as processing goes, it will always be true that as molecular weight decreases, viscosity decreases and the critical extrusion rate for melt fracture increases.

3.3.2 Molecular weight distribution

Most investigators (6, 47) of the influence of polydispersity of polymers on melt fracture find that critical stress is independent of polydispersity, but Mills et al. (27) find, for high-density polyethylene, that as polydispersity widens, the critical stress is increased. So far as the critical rate is concerned, there will generally be a considerable increase with increasing width of distribution.

4. CAPILLARY FLOW

4.1 Theory

The basic equations which describe the flow of a fluid in a capillary are the equations of continuity, momentum, and energy, which are mathematical formulations of fundamental physical principles of conservation of mass, momentum and energy, respectively. These equations in their most general form are:

Continuity equation—

$$\frac{D\rho}{Dt} = -\rho(\nabla \cdot \bar{v}) \quad (4-1)$$

Momentum equation—

$$\left(\frac{D\bar{v}}{Dt}\right) = -\nabla P - (\nabla \cdot \bar{\tau}) + \sum_s \rho_s F_s \quad (4-2)$$

Energy equation—

$$\rho c_v \frac{DT}{Dt} = -(\nabla \cdot \bar{q}) - T \left(\frac{\partial P}{\partial T}\right)_\rho (\nabla \cdot \bar{v}) + (\bar{\tau} : \nabla \bar{v}) \quad (4-3)$$

The vector form in which the continuity, momentum and energy equations are written above has the advantage of making the equations concise and independent of coordinate systems. In analyzing flow problems, however, one must usually select a coordinate system and resolve the vector and tensor quantities into components. The choice of a coordinate system depends

primarily upon the geometry of the boundaries of the fluid.

The geometry of the problem and the coordinates used are given in Figure 3.

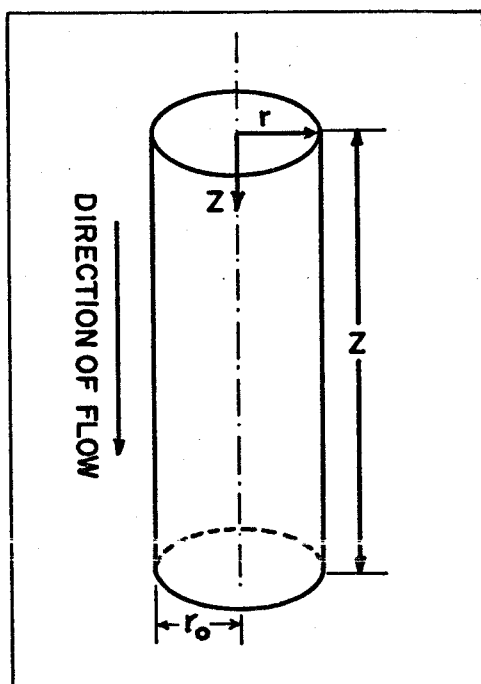


FIG. 3. SCHEMATIC ILLUSTRATION OF THE FLOW IN A CAPILLARY TUBE .

In cylindrical coordinates (r, θ, z) , equation (4-2) may be represented in terms of τ , by the following equations, assuming gravity to be the only field force present:

r-component—

$$\rho \left(\frac{\partial v_r}{\partial t} + v_r \frac{\partial v_r}{\partial r} + \frac{v_\theta}{r} \frac{\partial v_r}{\partial \theta} - \frac{v_\theta^2}{r} + v_z \frac{\partial v_r}{\partial z} \right) = -\frac{\partial p}{\partial r} - \left[\frac{1}{r} \frac{\partial}{\partial r} (r \tau_{rr}) + \frac{1}{r} \frac{\partial \tau_{r\theta}}{\partial \theta} - \frac{\tau_{\theta\theta}}{r} + \frac{\partial \tau_{rz}}{\partial z} \right] + \rho g_r \quad (4-4)$$

θ -component—

$$\begin{aligned} \rho \left(\frac{\partial v_\theta}{\partial t} + v_r \frac{\partial v_\theta}{\partial r} + \frac{v_\theta}{r} \frac{\partial v_\theta}{\partial \theta} + \frac{v_r v_\theta}{r} + \frac{v_z \partial v_\theta}{\partial z} \right) = \\ = - \frac{1}{r} \frac{\partial p}{\partial \theta} - \left[\frac{1}{r^2} \frac{\partial}{\partial r} (r^2 \tau_{r\theta}) + \frac{1}{r} \frac{\partial \tau_{\theta\theta}}{\partial \theta} + \frac{\partial \tau_{\theta z}}{\partial z} \right] + \rho g_\theta \quad (4-5) \end{aligned}$$

z -component—

$$\begin{aligned} \rho \left(\frac{\partial v_z}{\partial t} + \frac{v_r \partial v_z}{\partial r} + \frac{v_\theta}{r} \frac{\partial v_z}{\partial \theta} + \frac{v_z \partial v_z}{\partial z} \right) = \\ = - \frac{\partial p}{\partial z} - \left[\frac{1}{r} \frac{\partial}{\partial r} (r \tau_{rz}) + \frac{1}{r} \frac{\partial \tau_{\theta z}}{\partial \theta} + \frac{\partial \tau_{zz}}{\partial z} \right] + \rho g_z \quad (4-6) \end{aligned}$$

The shear rate dv_z/dr is always negative, since r is measured from the center line, and τ_{rz} is always positive. i.e., the momentum is transferred from the center line towards the wall. Therefore, to define an apparent viscosity which will not be constant, we have

$$\tau_{rz} = -\eta_a \left(\frac{dv_z}{dr} \right) \quad (4-7)$$

where η_a is the true apparent viscosity.

For the purpose of mathematical development the following assumptions are made:

1. The flow is steady (all partial derivatives with respect to time are zero).
2. The axial component of the velocity (v_z) is assumed to be a function of the radial distance r alone. The radial and tangential components (v_r, v_θ) of the velocity are assumed

zero. (V_r is assumed to be negligible in comparison to V_z , and V_θ is zero because of axial symmetry.)

3. End effects are neglected with respect to the development of the velocity profile.
4. External forces, such as gravity, are neglected.
5. Laminar flow prevails throughout.
6. There is no slip at the walls.
7. The non-Newtonian nature of the fluid can be taken into account by using the ordinary Newtonian expression for the momentum flux, but with the coefficient of shear viscosity taken to be some assumed function of the local shear stress.
8. The flow is isothermal.

Then these assumptions are made, the equations (4-4) and (4-6) reduce to:

$$0 = -\frac{\partial p}{\partial r} - \frac{1}{r} \frac{\partial}{\partial r} (r\tau_{rr}) - \frac{\tau_{\theta\theta}}{r} \quad (4-8)$$

$$0 = -\frac{\partial p}{\partial z} - \frac{1}{r} \frac{\partial}{\partial r} (r\tau_{rz}) \quad (4-9)$$

From equation (4-9)

$$\frac{\partial}{\partial r} (r\tau_{rz}) = -\frac{\partial p}{\partial z} r dr$$

that is,

$$\tau_{rz} = -\frac{r}{2} \frac{dp}{dz} \quad (4-10)$$

At the wall, $r = r_0$ and $\tau_{rz} = \tau_w$

$$\tau_w = -\frac{r_0}{2} \frac{dp}{dz} \quad (4-11)$$

Dividing (4-10) by (4-11) we get:

$$\tau_{rz} = \frac{r}{r_0} \tau_w \quad (4-12)$$

The boundary condition is $V_z = 0$ at $r = r_0$ for no slip at the wall.

The volume flow rate in a laminar steady state flow through a circular tube or capillary of radius r_0 is related to the velocity $V_z(r)$ by:

$$Q = \int_0^{r_0} 2\pi r V_z(r) dr \quad (4-13)$$

We have from equation (4-12) that:

$$r = \frac{r_0 \tau_{rz}}{\tau_w}$$

Equation (4-13) becomes:

$$Q = 2\pi \left(\frac{r_0}{\tau_w} \right)^2 \int_0^{\tau_w} \tau_{rz} V_z d\tau_{rz} \quad (4-14)$$

The velocity may be given by:

$$V_z = \int_r^{r_o} \left(- \frac{dV_z}{dr} \right) dr$$

that is,

$$V_z = \frac{r_o}{\tau_w} \int_{\tau_{rz}}^{\tau_w} \left(- \frac{dV_z}{dr} \right) d\tau_{rz} \quad (4-15)$$

Combining equations (4-14) and (4-15) we have

$$Q = 2\eta \left(\frac{r_o}{\tau_w} \right)^3 \int_0^{\tau_w} \tau_{rz} \int_{\tau_{rz}}^{\tau_w} \left(- \frac{dV_z}{dr} \right) d\tau_{rz} d\tau_{rz}$$

that is,

$$\frac{4Q}{\eta r_o^3} = \frac{8}{\tau_w^3} \int_0^{\tau_w} \tau_{rz} \int_{\tau_{rz}}^{\tau_w} \left(- \frac{dV_z}{dr} \right) d\tau_{rz} d\tau_{rz} \quad (4-16)$$

Integrating by parts:

$$\frac{4Q}{\eta r_o^3} = \frac{4}{\tau_w^3} \int_0^{\tau_w} \tau_{rz}^2 \left(- \frac{dV_z}{dr} \right) d\tau_{rz} \quad (4-17)$$

Equation (4-17) is the general equation which relates the flow to the velocity gradient in the system.

For a Newtonian fluid $(-\frac{dV_z}{dr}) = \frac{\tau_{rz}}{\mu}$, and equations (4-15) and (4-16) integrate to:

$$V_z = -\frac{r_o^2}{4\mu} \frac{dp}{dz} \left(1 - \frac{r^2}{r_o^2}\right) \quad (4-18)$$

and

$$\Gamma = \frac{4Q}{\pi r_o^3} = \frac{\tau_w}{\mu} = -\frac{r_o}{2\mu} \frac{dp}{dz} \quad (4-19)$$

The latter equation can be used to define a capillary shear diagram as $\frac{4Q}{r_o^3}$ versus τ_w .

For a non-Newtonian fluid, it is possible to define an apparent viscosity as:

$$\frac{1}{\eta_{ap}} = \frac{4Q/\pi r_o^3}{\tau_w} = \frac{4}{\tau_w} \int_0^{\tau_w} \tau_{rz}^2 \left(-\frac{dV_z}{dr}\right) d\tau_{rz} \quad (4-20)$$

where η_{ap} may be distinguished from η_a as defined by equation (4-7), i.e.,

$$\tau_w = -\eta_a \left(\frac{dV_z}{dr}\right)_w = \eta_{ap} \left(\frac{4Q}{\pi r_o^3}\right)$$

The term $\Gamma = 4Q/\pi r_o^3$ is sometimes called the pseudo-shear rate.

Rabinowitsch (48) obtained a simple relation between the flow rate and the wall shear rate (or between η_a and η_{ap}). Differentiation of equation (4-17) gives:

$$\frac{d[\tau_w^3(4Q/\eta r_o^3)]}{d\tau_w} = 4\tau_w^2 \left(-\frac{dV_z}{dr}\right)_w \quad (4-21)$$

that is,

$$\frac{4Q}{\eta r_o^3} \cdot \frac{1}{4\tau_w^2} \cdot 3\tau_w^2 + \frac{\tau_w^3}{4\tau_w^2} \frac{d}{d\tau_w} \frac{4Q}{\eta r_o^3} = \left(-\frac{dV_z}{dr}\right)_w \quad (4-22)$$

$$\left(-\frac{dV_z}{dr}\right)_w = \frac{3}{4} \frac{4Q}{\eta r_o^3} + \frac{\tau_w}{4} \frac{d(4Q/\eta r_o^3)}{d\tau_w} \quad (4-23)$$

Equation (4-23) can now be used to obtain the basic shear diagram, i.e., for any given value of τ_w , the value of $4Q/\eta r_o^3$ may be obtained from the data, and the slope of the curve may also be obtained at the point, hence $\left(-\frac{dV_z}{dr}\right)_w$ may be calculated. Both τ_w and $\left(-\frac{dV_z}{dr}\right)_w$ are obtained at the same point and hence are the terms of the basic shear diagram. There is no need to assume any kind of rheological law for this calculation.

4.2 Errors in Capillary Flow

4.2.1 Slip at the wall

The equation (4-14) may be modified for slip-at-the-wall conditions by allowing for a slip velocity V_s : i.e., the new boundary condition at the wall becomes $V_z = V_s$ as opposed to $V_z = 0$. So,

$$V_z = V_s + \int_r^{r_o} \left(-\frac{dV_z}{dr}\right) dr$$

$$v_z = v_s + \frac{r_o}{\tau_w} \int_{\tau_{rz}}^{\tau_w} \left(- \frac{dv_z}{dr} \right) d\tau_{rz} \quad (4-24)$$

Combining equation (4-24) with equation (4-14) we have a relation similar to equation (4-16), that is,

$$\frac{4Q}{\eta r_o^3} = \frac{4v_s}{r_o} + \frac{8}{\tau_w^3} \int_0^{\tau_w} \tau_{rz} \int_{\tau_{rz}}^{\tau_w} \left(- \frac{dv_z}{dr} \right) d\tau_{rz} d\tau_{rz} \quad (4-25)$$

Integrating by parts, as before, we have an equation similar to equation (4-17)

$$\frac{4Q}{\eta r_o^3} = \frac{4v_s}{r_o} + \frac{4}{\tau_w^3} \int_0^{\tau_w} \tau_{rz}^2 \left(- \frac{dv_z}{dr} \right) d\tau_{rz} \quad (4-26)$$

Oldroyd (49) defines:

$$\zeta = \frac{v_s}{\tau_w} \quad \text{and} \quad \phi = \frac{4}{\tau_w} \int_0^{\tau_w} \tau_{rz}^2 \left(- \frac{dv_z}{dr} \right) d\tau_{rz}$$

Substituting the above relations into equation (4-26) we have:

$$\frac{4Q}{\eta r_o^3} = (4\zeta / r_o + \phi) \tau_w \quad (4-27)$$

A plot of $4Q/\eta r_o^3$ versus $1/r_o$ will determine both ζ and ϕ .

With this information we can then obtain the true basic shear diagram.

As can be seen from equation (4-27) at any constant τ_w , for a system with slip, increasing the diameter will decrease $4Q/\eta r_0^3$, but there is no effect of length if steady state is obtained. Hence, a plot of $4Q/\eta r_0^3$ versus τ_w will determine the existence or the absence of slip. If slip is present then the slip velocity may be easily determined from Oldroyd's parameters.

4.2.2 End effects

This analysis of flow in a capillary, described in section (4.1) is based upon the assumption that a simple shear flow exists. This is achieved in steady state, laminar, isothermal flow in a tube of constant cross section, as long as one does not consider regions near the entrance and exit of the tube. If these end effects cause an appreciable amount of pressure drop, the estimation of τ_w by equation (4-10) is in error.

The accuracy in calculating the end effects for pipe flow is far from satisfactory, even for Newtonian materials. The treatment is complicated by the fact that pressure-drop measurements are usually made between two reservoirs, and thus, there may be both an upstream entrance effect and a downstream exit effect. These in turn involve frictional losses and kinetic energy corrections associated with the change in velocity and the development of the velocity profile. It is preferable to design a capillary instrument so that end effects are negligible. But this is not always possible, for the case of molten polymers.

It will prove convenient in the discussion to refer to the various regions shown in Figure (4). Region 3 is designated the region of steady flow. The development of the steady flow velocity profile occurs in region 2, the entrance region. The length of tube required for the complete development of the steady flow velocity profile is designated as Le . This length is generally a function of tube diameter and some dynamic parameters. For example, for Newtonian fluids, the "entrance length" depends upon the Reynolds number (4)

$$Le/D = 0.035 \frac{v_m \rho v_c}{\eta} = 0.035 R_e$$

where R_e represents the Reynolds number for the flow in the tube.

Obviously, if one applies the equations developed for region 3 to the over-all tube, the entrance region will introduce certain errors.

One method of minimizing the effect of the entrance length is to use a viscometer tube so long that the pressure drop over the entrance region is very small compared with the drop over the entire tube. This means that if L is the total tube length, then Le/L must be small, perhaps of the order of 0.01. Because of the high viscosity of polymer melts, however, it is difficult to work with long capillaries.

An empirical method of correcting for entrance effects has been developed by Bagley (50). In Bagley's technique, the equation for shear stress is modified by assuming that the

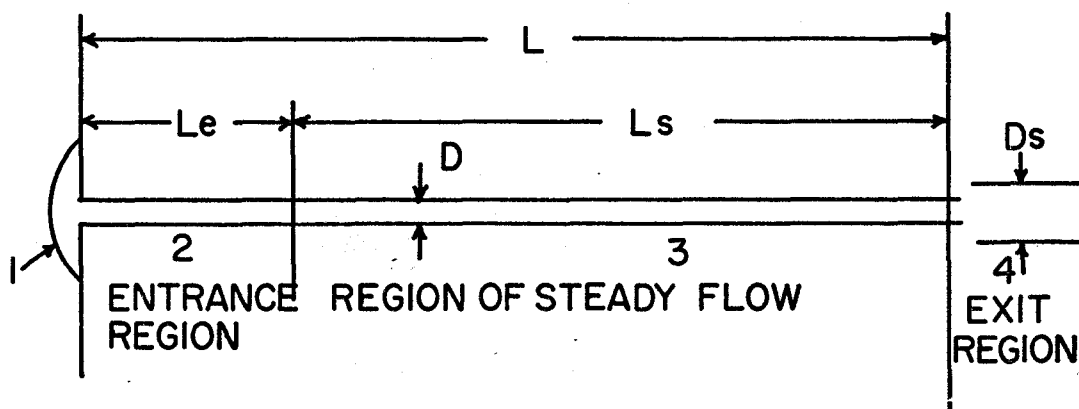


FIG. 4. REGIONS ASSOCIATED WITH FLOW THROUGH TUBES.

entrance effect is a function of the capillary dimensions. If experimental data from a series of capillaries are available, the correction term can be obtained by extrapolating to zero pressure the linear plot of pressure versus L/D (at constant shear rate). This correction term is strongly dependent on the shear rate and it also varies from one polymer to another. If the correction terms are determined and the shear stresses re-calculated, flow data from different capillaries reduce to a single curve.

The procedure developed by Bagley is outlined below (4). In the entrance region, fluid particles entering the tube from the reservoir are accelerated to their final steady flow velocities. The energy consumed in this process causes the pressure to drop more rapidly in this region than in the steady flow region. As shown by Figure 5, the pressure gradient decreases throughout the length L_e of the entrance region and eventually reaches a constant value that is maintained over the length L_s of the steady flow region.

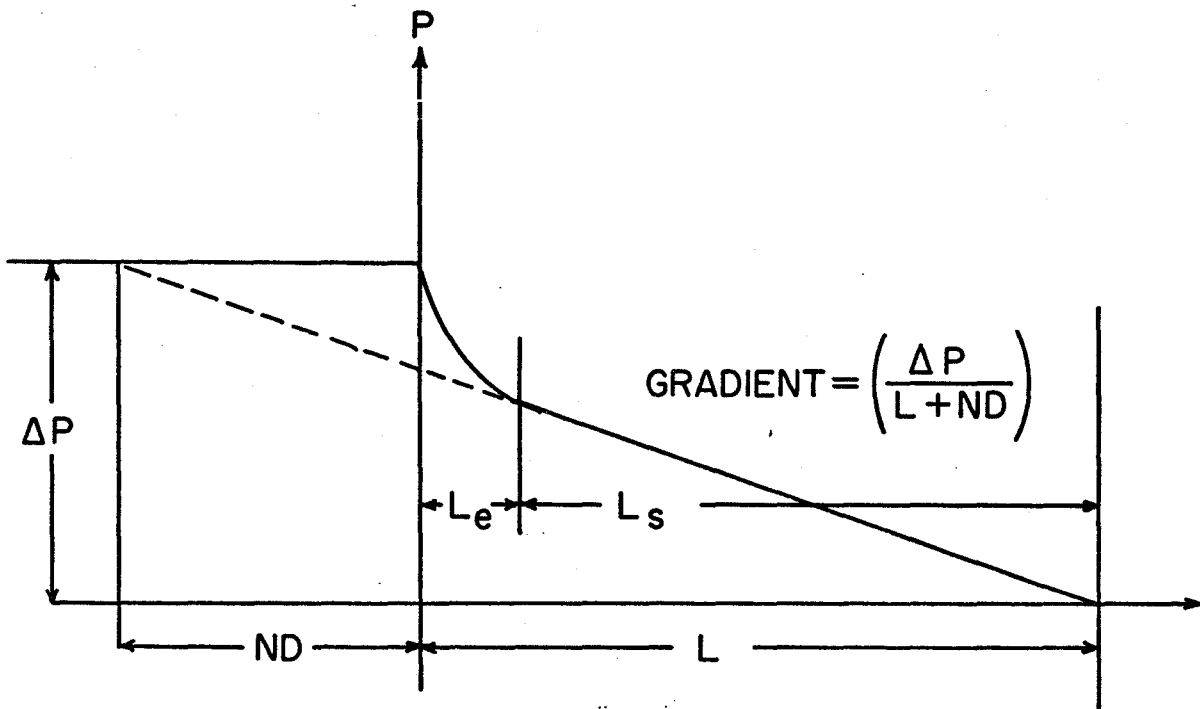


FIG.5. CORRECTION OF THE TUBE LENGTH BY THE ADDITION OF LENGTH ND IN ORDER TO CALCULATE THE PRESSURE GRADIENT.

In the steady flow region the shear rate $\dot{\gamma}_w$ at the tube wall can be calculated with equation (4-23) if the shear stress τ_w at the tube wall is known. Hence, the entrance correction problem is essentially one of determining the true value of τ_w from the over-all measurements of flow rate and pressure drop.

Noting from equation (4-23) that τ_w is a unique function of the parameter $\Gamma = 4Q/\pi r_o^3$, we have

$$\tau_w = D/4 P_s = g(\Gamma) \quad (4-28)$$

where P_s is the pressure gradient in the region of steady flow.

It is clear that

$$P_s = \left(\frac{\Delta P}{L+ND} \right) \quad (4-29)$$

where ND , as shown by Figure 5, represents a fictitious tube length, that when added to the actual length enables one to use the over-all pressure drop in calculating the gradient in the steady flow section.

The expression for the shear stress at the wall in the steady flow section of the tube (equation (4-29)) can now be written

$$\tau_w = \frac{D}{4} \left(\frac{\Delta P}{L+ND} \right) = f(\Gamma) \quad (4-30)$$

Upon rearranging, equation (4-30) becomes

$$\frac{L}{D} = -N + \frac{\Delta P}{4f(\Gamma)} \quad (4-31)$$

which suggests that the value of N might be determined from flow measurements made with a series of capillary tubes having different L/D ratios. For each tube, the pressure drop ΔP , giving some specific value of $\Gamma = 4Q/\eta r_0^3$, would be determined. Then, by plotting L/D versus ΔP , a straight line having $-N$ as an intercept would be obtained, and from equation (4-30) corrected values of shear stress would be calculated.

4.2.3 Heat effects

Deformation gives rise to frictional forces within the fluid, and this friction dissipates a part of the kinetic energy of the fluid and causes it to appear as heat. This generation of heat can lead to significant temperature variations across the shear fields. One concludes from this that no flow is isothermal, despite any precautions of thermostating the boundaries of the system.

Because fluid properties such as viscosity are rather strongly temperature dependent the shear stress-shear rate relation is considerably altered by non-isothermal effects. Hence, a shear stress-shear rate curve obtained under non-isothermal conditions does not reflect the basic fluid response independently of any temperature-dependent effect. In this case, one must be able to correct any calculations based on an isothermal analysis and separate that part of the response due

to non-isothermal behaviour from that part of the response due to non-Newtonian behaviour. This would require a knowledge of the temperature field in the fluid as well as a knowledge of the effect of temperature on fluid properties such as viscosity.

Let us now consider the application of the basic flow equations to the problem of the extrusion of molten polymers through small capillary tubes of circular cross section at such high shear rates that the heat produced by viscous dissipation is of importance (4). The same assumptions are made as in section 4.1, but now we allow for changes in density and temperature of the fluid. So equations (4-1), (4-3), (4-6), become:

$$\rho \left(\frac{\partial v_z}{\partial z} \right) + v_z \left(\frac{\partial \rho}{\partial z} \right) = 0 \quad (4-32)$$

$$\rho v_z \left(\frac{\partial v_z}{\partial z} \right) = - \left(\frac{\partial P}{\partial z} \right) + \frac{1}{r} \frac{\partial}{\partial r} \left[r \eta_a \left(\frac{\partial v_z}{\partial r} \right) \right] \quad (4-33)$$

$$\rho C_v v_z \left(\frac{\partial T}{\partial z} \right) = \frac{K}{r} \frac{\partial}{\partial r} \left[\left(r \frac{\partial T}{\partial r} \right) \right] + K \left(\frac{\partial^2 T}{\partial z^2} \right) - T \left(\frac{\partial P}{\partial T} \right) \rho \left(\frac{\partial v_z}{\partial z} \right) + \eta_a \left(\frac{\partial v_z}{\partial r} \right)^2 \quad (4-34)$$

The boundary conditions are:

$$T = T_0 \quad \text{at} \quad z = 0$$

$$\frac{\partial T}{\partial r} = 0 \quad \text{at} \quad r = 0$$

$$T = T_0 \quad \text{at} \quad r = r_0$$

where T_0 is the reservoir temperature of the fluid, and K , ρ , and C_v are the fluid thermal conductivity, density, and heat capacity, respectively.

The total differential of the fluid density ρ , is written

$$d\rho = \left(\frac{\partial \rho}{\partial T}\right)_P dT + \left(\frac{\partial \rho}{\partial P}\right)_T dP \quad (4-35)$$

which can be put in the equivalent form

$$d\rho = -k\rho dT + b\rho dP \quad (4-36)$$

by introducing the quantities k , and b , where k is the coefficient of thermal expansion and b the compressibility of the fluid. These quantities are defined by the equations

$$k = -\frac{1}{\rho} \left(\frac{\partial \rho}{\partial T}\right)_P$$

$$b = \frac{1}{\rho} \left(\frac{\partial \rho}{\partial P}\right)_T \quad (4-37)$$

From equation (4-36) it can be shown that

$$\left(\frac{\partial P}{\partial T}\right)_\rho = \left(\frac{k}{b}\right) \quad (4-38)$$

To consider the variation of the fluid density with the z position coordinate, equation (4-36) is written

$$\left(\frac{\partial \rho}{\partial z}\right) = -k\rho \left(\frac{\partial T}{\partial z}\right) + b\rho \left(\frac{\partial P}{\partial z}\right) \quad (4-39)$$

and upon introducing (4-39) into the equation of continuity (4-32) one obtains

$$\frac{\partial v_z}{\partial z} = v_z \left[k \left(\frac{\partial T}{\partial z} \right) - b \left(\frac{\partial P}{\partial z} \right) \right] \quad (4-40)$$

If one now introduces (4-38) and (4-40) into the equation of momentum and energy (4-33) and (4-34) one obtains

$$\rho v_z^2 \left[k \left(\frac{\partial T}{\partial z} \right) - b \left(\frac{\partial P}{\partial z} \right) \right] = - \left(\frac{\partial P}{\partial z} \right) + \frac{1}{r} \frac{\partial}{\partial r} \left[r \eta_a \left(\frac{\partial v_z}{\partial r} \right) \right] \quad (4-41)$$

$$\rho c_v v_z \left(\frac{\partial T}{\partial z} \right) = \frac{K}{r} \frac{\partial}{\partial r} \left[r \left(\frac{\partial T}{\partial r} \right) \right] + K \left(\frac{\partial^2 T}{\partial z^2} \right) - T k v_z \left[\frac{k}{b} \left(\frac{\partial T}{\partial z} \right) - \left(\frac{\partial P}{\partial z} \right) \right] + \eta_a \left(\frac{\partial v_z}{\partial r} \right)^2 \quad (4-42)$$

Equations (4-41) and (4-42) constitute a pair of simultaneous non-linear, partial differential equations. Solutions of certain special cases of these equations have been obtained. For example, if the fluid properties are assumed constants, in which case the isothermal velocity profile is known, solutions exist from which the temperature profile may be calculated as a function of axial position. Bird (15) gives solutions for the case of the power law fluid with either the isothermal or adiabatic wall. Toor (51) solves a similar problem but allows for compressibility of the fluid and its accompanying heating or cooling effect. Siegel et al. (52)

gives solutions for the Newtonian fluid with boundary conditions specifying constant prescribed flux at the tube wall. The simplest case studied was that of Brinkman (53), for the Newtonian fluid with temperature-independent properties, with either isothermal or adiabatic wall.

None of the studies named accounts for the alteration of the flow field arising from viscosity variation across the radius of the capillary and so none of these studies may be used to correct viscometry data. The major use of the results of these workers is the estimation of the temperature rise experienced by the fluid. Capillary viscometry of highly viscous materials should always be accompanied by an estimate of temperature rise due to viscous heating. If the estimate of the maximum temperature rise is small, say from 1°C , then one might judge that the results need not be corrected at all for heating effects. If the estimated temperature rise is large, then one is faced with the problem of rejecting the data or accepting the results as subject to significant error.

In order to calculate the temperature rise due to viscous heating, in our experiments we used a nomograph that has been prepared by Middleman (54). This nomograph yields the wall temperature at the outlet of a capillary (or at any axial position in the capillary) and it is based upon Bird's solutions for the power law fluid with adiabatic wall. (Experimental results (55) indicate that the wall of a capillary behaves in a nearly adiabatic manner under usual operating

conditions.) Figure 6 shows Bird's solutions, plotted as a dimensionless wall temperature as a function of a dimensionless axial variable with n as parameter. The dimensionless variables are defined as:

$$\theta_o = (T - T_o) \frac{4Kk_o^{1/n}}{D^2 \tau_w^{(n+1)/n}} \left(\frac{3n+1}{2n} \right)^2 \quad (4-43)$$

$$Z_o = \frac{4}{P_e'} \frac{n+1}{3n+1} \frac{z}{D} \quad (4-44)$$

where τ_w is the wall shear stress (for our experiments the corrected shear stress) and P_e' is the Pe'clet number $P_e' = D V_m \rho C_p / K$. This nomograph neglects the effect of non-Newtonian flow in that the value $n - \frac{1}{2}$ has been used in the approximations. In cases tested by Middleman (54) it was found to be accurate to within a factor of 2, in comparison with the use of the exact relationships.

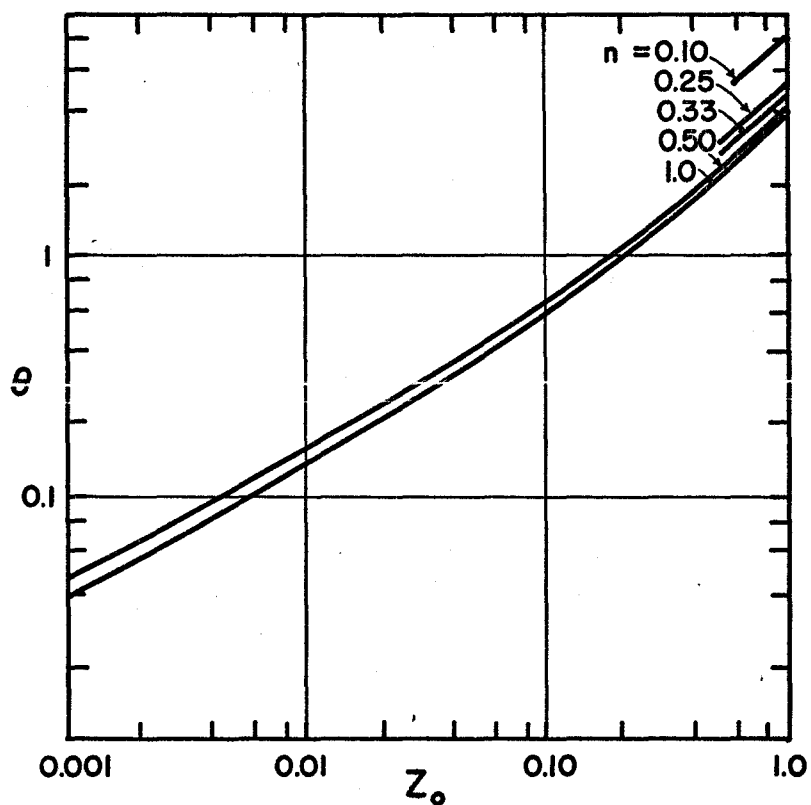


FIG. 6. DIMENSIONLESS WALL TEMPERATURE RISE DOWN THE LENGTH OF A CAPILLARY DUE TO VISCOUS HEATING.

The nomograph shown in figure 7 is based upon the solution for fully developed capillary flow of a power law fluid (15). That solution gives the temperature rise at the wall of the capillary at some axial position z , under the assumption that the wall is adiabatic. To simplify the nomograph, approximations were made which essentially remove any dependence on the power law index n . In examples tested, the nomograph yields a temperature rise within a factor of 2 of the analytical solution. Hence, it provides a rapid estimate of the order of magnitude of the effect of viscous dissipation in a highly viscous capillary flow.

All scales are in cm/g/sec units. A short table of thermal properties of polystyrene is also given. Note especially, that k must be in cm/gm/sec units.

Move from left to right across the nomograph. For a given set of data, begin by connecting points on the $\dot{\gamma}$ and τ scales, and find the intersection of this line with Reference scale 1. Connect that point, through D, to Reference scale 2, and so on across the other scales to the temperature scale. The value of ΔT is an estimate of the temperature rise at the wall of the capillary, at the given value of z/D .

Thermal Properties

	$K \left(\frac{\text{g. cm}}{\text{sec}^3 \text{ } ^\circ\text{C}} \right)$	$K/\rho C_V \left(\frac{\text{cm}^2}{\text{sec}} \right)$
Polystyrene	1.2×10^4	6.2×10^{-4}

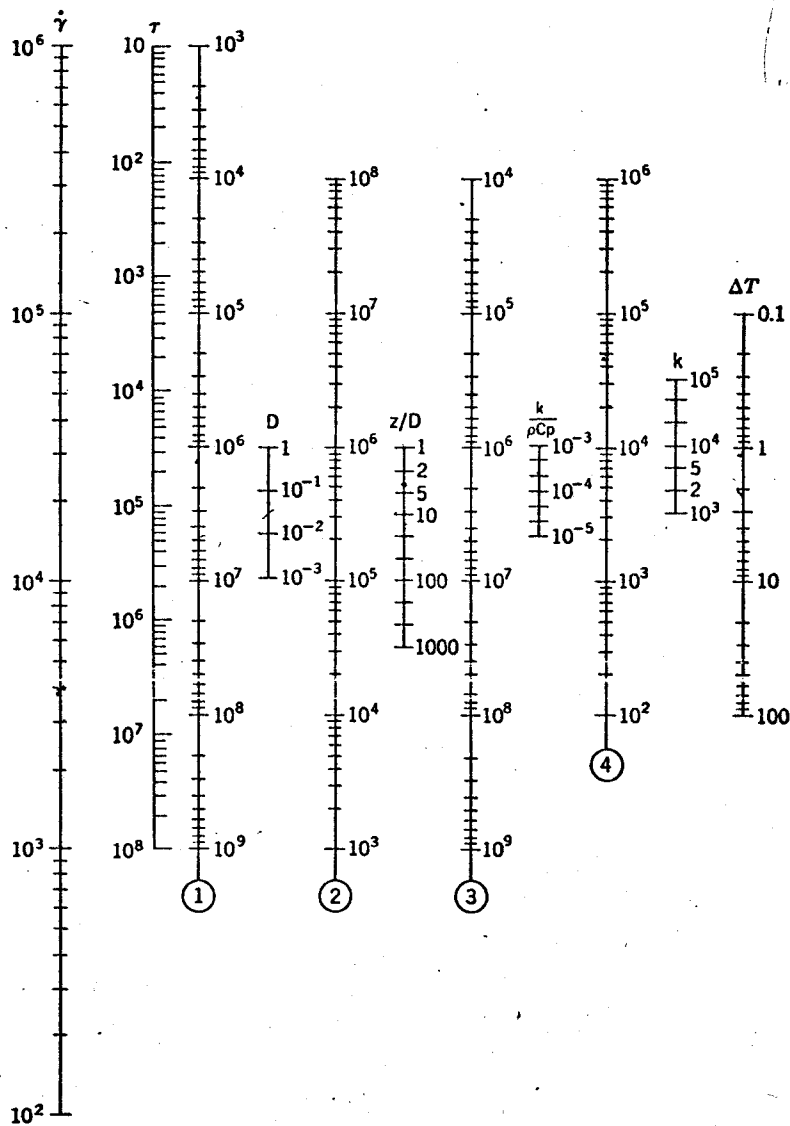


Fig. 7. Nomograph for Estimation of Temperature Rise due to Viscous Dissipation.

4.2.4 Laminar flow

The flow of molten polymers is usually laminar. Because of their high viscosity one cannot reach the critical value of Reynold's number where turbulent flow is encountered.

4.2.5 Expansion of the fluid

The correction for the fluid expansion along the capillary changes the value of Q . For polystyrene one can calculate this correction from the equation of state of the fluid as given by a Van der Waals type equation (56):

$$(V - 0.882) (p + 27,000) = 11.6T \quad (4-45)$$

where V is the specific volume in cm^3/g , p the pressure in psi and T the absolute temperature. Differentiating, one has

$$\left(\frac{\partial V}{\partial p}\right)_T = - 11.6T / (p + 27,000)^2 \text{ cm}^3/\text{g.psi} \quad (4-46)$$

If the pressure drop is linear along the capillary, by measuring Q (and hence $\dot{\gamma}_w$) halfway along the capillary, one has to correct Q by the following amount:

$$\frac{p(\partial V/\partial p)_T}{2} \quad (4-47)$$

where p is the extruding pressure in psi.

4.3 Normal Stress Effects

To this point, the analysis of capillary flow has been limited to the measurement of the shear stresses, or the corresponding forces, required to maintain a simple shear flow in a capillary tube. It is known, however, that many fluids, when subjected to a simple shear flow, develop not only shear stresses but also normal stresses. The normal stresses are associated with both the static pressure P and a normal shear. For steady state capillary flow the normal stresses are (57):

$$P_{rr} = -p + \tau_{rr} \quad (4-48)$$

$$P_{\theta\theta} = -p + \tau_{\theta\theta} \quad (4-49)$$

$$P_{zz} = -p + \tau_{zz} \quad (4-50)$$

In order to generate information specifically about the dynamic stress components, it is necessary to "remove" the influence of p from the measurement. This is most commonly achieved by presenting results in terms of stress differences. So, for equations (4-48), (4-49), (4-50), we have:

$$P_{zz} - P_{\theta\theta} = \tau_{zz} - \tau_{\theta\theta} = \tau_{zz} = \sigma_1 \quad (4-51)$$

$$P_{rr} - P_{\theta\theta} = \tau_{rr} - \tau_{\theta\theta} = \tau_{rr} = \sigma_2 \quad (4-52)$$

where all stresses are a function of both r and z , that is, $P_{zz}(r,z)$. It is by no means easy to evaluate the normal stress

terms, and there is considerable disagreement on how measured variables are to be translated into meaningful results (5, 58, 59, 60). The first capillary jet experiments reported were by Philippoff and Gaskins (38, 61, 62).

The term σ_2 can be evaluated from a detailed knowledge of the conditions within the capillary tube. From the equation (4-8) we obtain

$$0 = - \left(\frac{\partial p}{\partial r} \right) - \left(\frac{\partial \tau_{rr}}{\partial r} \right) - \left(\frac{\tau_{rr}}{r} \right) - \left(\frac{\tau_{\theta\theta}}{r} \right)$$

or

$$\frac{\partial p_{rr}}{\partial r} = - \left(\frac{\tau_{rr} - \tau_{\theta\theta}}{r} \right) = - \frac{\sigma_2}{r} \quad (4-53)$$

Integration of this between 0 and r gives

$$p_{rr}(r, z) - p(0, z) = - \int_0^r \sigma_2 d \ln r \quad (4-54)$$

since by symmetry at the tube axis, $\tau_{rr}(0, z) = 0$. At the exit of the tube $z = L$, and at the wall $r = r_0$. Thus,

$$p_{rr}(r_0, L) = p(r_0, L) - \int_0^{r_0} \sigma_2 d \ln r \quad (4-55)$$

Differentiating with respect to $\ln \tau_w$ and using the linear variation of τ_w over the radius (equation 4-12) gives:

$$\frac{dp(r_0, L)}{d \ln \tau_w} = - \sigma_2 \left(\frac{r_0}{\tau_w} \right)^2 + \frac{dp(0, L)}{d \ln \tau_w} \quad (4-56)$$

The expression $\sigma_2(\dot{\gamma}_w^2)$ means that σ_2 will be a unique function of the square of the shear rate at the wall, $(\dot{\gamma})_w^2$. Sakiadis (63) assumed that the last term was zero because the system was open to the atmosphere; that is, at the center line, the stresses are zero by symmetry and only the pressure exists. This is taken as the ambient pressure P_0 and does not change.

$$\frac{dp(r_0, L)}{d \ln \dot{\gamma}_w} = \frac{dp_0}{d \ln \dot{\gamma}_w} = 0$$

Sakiadis then obtained a non-zero σ_2 . White (60) has criticized Sakiadis' use of equation (4-56) for his data, so these results are open to question.

The term σ_1 can be evaluated from an integral momentum balance written for the jet issuing from a capillary tube.

This takes the form

$$\int_0^{r_0} 2\eta r \rho V_z^2 dr - \int_0^{r_0} 2\eta r P_{zz} dr + \eta r (r_j - r_0) - \eta r_0^2 p_0 = \eta r_j^2 \rho V_j^2 = \rho Q^2 / \eta r_j^2 \quad (4-57)$$

where the subscript j refers to the jet and p_0 is the ambient pressure, usually taken as zero, without loss of generality. The third term accounts for surface tension effects, and is probably small at high exit velocities (58). This assumption is usually made in data evaluation (60, 64). It is easiest to assume a power law for V_z and differentiate equation (4-57)

to obtain an expression for $P_{zz}(r_0, L)$ in terms of the surface tension contribution and terms involving the jet contraction or expansion ratio (64). An equivalent approach (60, 63) is to use equations (4-51), (4-52) to give

$$P_{zz}(r, z) - P_{rr}(r, z) = \sigma_1 - \sigma_2$$

then combine this with equation (4-54) to obtain

$$P_{zz}(r, z) = p(o, z) - \int_0^r \sigma_2 d \ln r + \sigma_1 - \sigma_2 \quad (4-58)$$

At the wall, equation (4-58) becomes

$$P_{zz}(r_0, L) = p(o, L) + \sigma_1(\dot{\gamma}_w^2) - \sigma_2(\dot{\gamma}_w^2) - \int_0^{r_0} \sigma_2 d \ln r \quad (4-59)$$

or, if we use equation (4-55) we obtain

$$P_{zz}(r_0, L) = p(r_0, L) + \sigma_1(\dot{\gamma}_w^2) - \sigma_2(\dot{\gamma}_w^2) \quad (4-60)$$

Sakiadis (63), in effect, neglects $P_{zz}(r_0, L)$ in equation (4-60) and calculates σ_1 from σ_2 obtained from equation (4-56) and the pressure $p(r_0, L)$. Because of existing questions of this measurement, White also questioned the use of equation (4-60) to interpret the data as measured.

Gavis and Middleman (58) have considered the source for the axial normal stress P_{zz} , concluding that there is, in addition to the internal normal stress, a profile relaxation

stress occurring outside the tube. The profile relaxation stress occurs in any fluid and is associated with the change in the velocity profile from that within the tube to the flat profile in the jet. The external normal stress develops in viscoelastic materials because of the change in the rate of shearing during the velocity profile relaxation (an elastic reaction to the change). Of course there is also the effect of surface tension or surface traction. Clearly, the simple jet is a complicated tool and measurements should be made with caution; it is not surprising that there are differences reported in the literature (63, 65). Savins (59), as still another alternative, has suggested the use of a pitot tube within the pipe to obtain a measure of

$$P_{zz}(r,z) + \frac{1}{2}\rho V_z^2$$

and thus, by equation (4-58), to obtain information and σ_1 and σ_2 .

5. EXPERIMENTAL WORK

5.1 Apparatus

The equipment used in this study was a capillary rheometer (melt indexer) purchased from Monsanto Research Corporation, which is shown in Figure 8 and consists of the following:

1. Rheometer ram stand with pressure gauges
2. Rheometer extruder barrel
3. Temperature controller cabinet.

Nitrogen was supplied in the piston from commercial cylinders in the range of 0 to 150 psi. The desired range of pressures were obtained through the dual-stage pressure regulator and accurately measured by the Rheometer's gauges. The barrel is a stainless steel cylinder having three heater bands (top, middle and bottom) wrapped directly around the barrel, spaced evenly along its length. By means of a retaining nut, orifices of different dimensions can be installed at the bottom of the barrel. The geometrical characteristics of the capillaries used are shown in Table I. The temperature controller unit was operated over a temperature range of 170°-250°C and could be controlled to about $\pm 1^\circ\text{C}$ at any temperature in this range.

The procedure followed during a run was as follows:

1. With the rheometer at test temperature, (with piston and oriface in place), about 10 gr of polymer were packed into

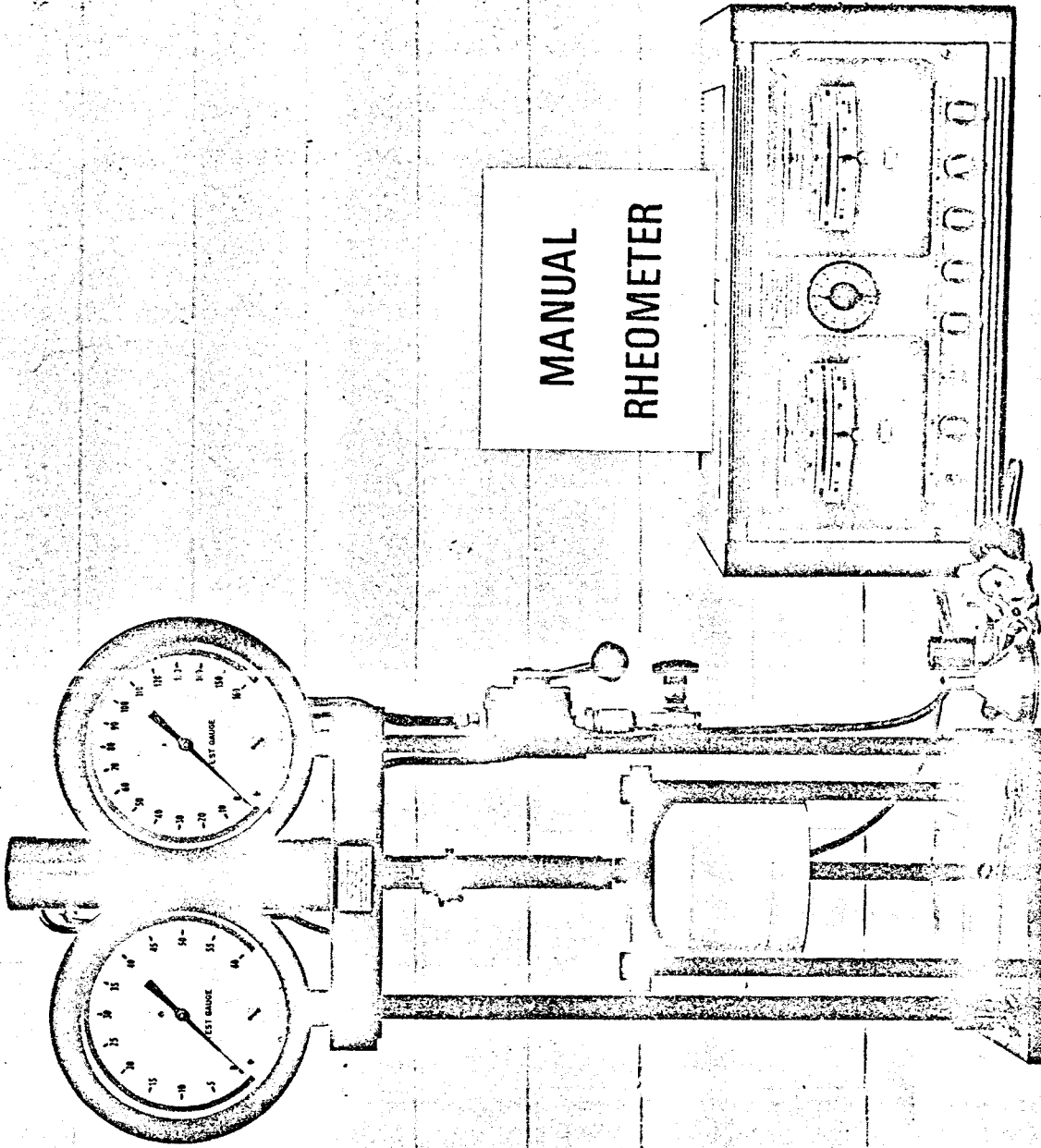


Figure 8 Manual Rheometer

Table I Diameters and Length/Diameter
Ratios of Capillary Tubes

Capillary no.	Entrance Angle	Diameter cm	L/D
1	60°	0.172	10
2	60°	0.104 ✓	15
3	60°	0.0812 ✓	19.5
4	60°	0.071	24

- the barrel incrementally to minimize air entrapment.
2. Sufficient time was allowed to elapse (about 45 minutes) to insure that the material was at the desired temperature.
 3. After the preheated time had elapsed, one inch of piston motion was extruded. Usually the first sample contained air bubbles and was discarded. When a steady flow had been obtained, the extrusion rate was determined by weighing samples of the extrudate collected over timed intervals.
 4. A higher pressure was then built up through the dual pressure regulator, and the above process was repeated to obtain data at a second pressure. In this way, data were obtained for extrusion rates at a series of driving pressures but at a constant temperature and the same polymer (and of course the same capillary). The incipience of fracture was visually determined by the appearance of a pronounced waviness in the extrudate. For polymers samples with M_w under 400,000, the extrudate was smooth and straight right up to the critical shear stress. For molecular weights above 400,000 the extrudates showed a loss of surface gloss and a mild surface roughness (sharkskin) before critical conditions were reached, both for narrow and broad distribution samples.

After the completion of the experiment, the remainder of the specimen was discharged and the orifice was pushed out through the top of the cylinder. The orifice was cleaned by dissolving the residue in a solvent (THF). A new orifice was adjusted and

the barrel was charged with a new polymer sample. This procedure was followed for all the samples used.

5.2 Materials

Five polystyrenes of narrow molecular weight distribution were obtained from the Pressure Chemical Co., Pittsburgh, Pa. They ranged in reported \bar{M}_w/\bar{M}_n from 1.06 to 1.20. Nine broad distribution polystyrenes were prepared by blending of fractions of narrow molecular weight distribution polystyrenes. The blending of fractions was done by dissolving components in tetrahydrofuran (at room temperature), then precipitating and filtering with purified methanol. The molecular weights of blends were calculated from the equations:

$$\bar{M}_w = \sum_i w_i (M_w)_i \quad (5-1)$$

$$\bar{M}_n = \frac{1}{\sum_i \frac{w_i}{(M_n)_i}} \quad (5-2)$$

$$\bar{M}_z = \frac{\sum_i w_i M_i^2}{\sum_i w_i M_i}$$

$$\bar{M}_{z+1} = \frac{\sum_i w_i M_i^3}{\sum_i w_i M_i^2}$$

where w_i is the weight fraction of the i component.

The characteristics of the materials used are listed in Table II.

Table II Polymer Samples Used

\bar{M}_w	$\frac{\bar{M}_w}{\bar{M}_n}$	$\frac{\bar{M}_z \bar{M}_{z+1}}{\bar{M}_w^2}$	Sources of Sample
97,200	< 1.06	1.25	Pressure Chemical Company
128,000	2.9	2.86	Blend 20,400 (0.40) + 200,000 (0.60)
200,000	< 1.06	1.25	Pressure Chemical Company
204,430	6.9	9.02	Blend 20,400 (0.65) + 498,000 (0.25) + 670,000 (0.10)
207,250	9.21	85.6	Blend 20,400 (0.895) + 1,800,000 (0.105)
207,300	2.78	6.15	Blend 51,000 (0.65) + 498,000 (0.35)
212,000	2.71	5.69	Blend 51,000 (0.60) + 200,000 (0.06) + 498,000 (0.34)
355,000	2.92	—	Monsanto Research Serial DD-0353
498,000	< 1.20	1.25	Pressure Chemical Company
600,000	2.32	8.42	Blend 200,000 (0.75) + 1,800,000 (0.25)
670,000	< 1.10	1.25	Pressure Chemical Company
760,000	2.60	5.76	Blend 200,000 (0.65) + 1,800,000 (0.35)
1,060,000	2.31	3.10	Blend 200,000 (0.30) + 498,000 (0.20) + 1,800,000 (0.50)
1,350,000	2.14	2.08	Blend 200,000 (0.20) + 498,000 (0.10) + 1,800,000 (0.70)
1,800,000	< 1.20	1.25	Pressure Chemical Company

5.3 Treatment of Data

In the present work, two macroscopic variables were measured: the pressure drop ΔP in the capillary rheometer and the volume flow rate Q . The pressure drop in the capillary rheometer is actually the sum of the following:

1. Pressure drop in capillary
2. Pressure drop in reservoir
3. Friction between piston and reservoir wall
4. Compressibility of melt.

Without loss of accuracy, the observed pressure was considered to be the pressure drop through the capillary. Any other losses were lumped into the entrance effect.

Apparent shear stress and pseudo-shear rate at the wall were calculated from these two quantities by using equations (4-11) and (4-19). Corrected values of shear stress (Bagley's entrance correction) and shear rate (Rabinowitsch correction) were obtained with the help of equations (4-30) and (4-23).

In addition to these two quantities, the expansion ratio D_s/D was also measured. (D_s is the diameter of the emerging polymer from the capillary. D is the diameter of the capillary tube.) Although this last quantity was not used in the analysis, it has been measured for future reference.

In Chapter 4 the errors encountered in a capillary flow were discussed. No further corrections were made because:

1. The flow was laminar. A maximum value of $Re = 10^{-2}$ was calculated at the incipience of fracture.

2. The flow was isothermal. A maximum temperature rise of 2°C was calculated, and so corrections for heat effects were considered negligible.
3. The compressibility of polymer was negligible as calculated from equations (4-46) and (4-47).

6. RESULTS AND DISCUSSION

The results of the experimental measurements, i.e., values of ΔP , τ_{ap} , $4Q/\pi r_o^3$, τ_w , $\dot{\gamma}_w$, D_s/D are given in Appendix I. Typical flow curves for monodisperse polystyrene with $\bar{M}_w = 670,000$ at 250°C are shown in Figures (9), (10), (11), (12), (13). Figure (9) shows the uncorrected flow curves for different capillaries with $L/D = 10, 15, 24$, while Figure (12) shows true shear stress τ_w versus shear rate $\dot{\gamma}_w$. Table III summarizes values of τ_{cr} , $\dot{\gamma}_{cr}$, η_{cr} , η_o and $\tau_{cr} \times \bar{M}_w$. Values of τ_{cr} , $\dot{\gamma}_{cr}$, η_{cr} were directly measured. Values of η_{cr} vs. $\dot{\gamma}$ were also obtained. However, estimations of η_o by extrapolation from high shear rates are subject to large errors. For this reason η_o was determined using the formula (66):

$$\log \eta_o = 3.4 \log Z + 2.7 \times 10^{16}/T^6 - 9.51 \quad (6-1)$$

where $Z = \bar{M}_w/52$.

From the experimental part of this work, one may observe:

1. The critical shear stress is independent of the capillary dimensions if end corrections are applied.
2. The critical shear stress varies between $.68 \times 10^6$ dynes/cm² and 2.15×10^6 dynes/cm². The product $\tau_{cr} \times \bar{M}_w$ ranges from 1.88×10^{11} to 12.9×10^{11} , and the ratio η_{cr}/η_o takes values from 0.0007 to 0.055. These results are therefore in contradiction with Spencer and Dillon's (2) and Bagley's (37) conclusion that $\tau_{cr} \times \bar{M}_w$ is a constant. Also Barto's (67) cri-

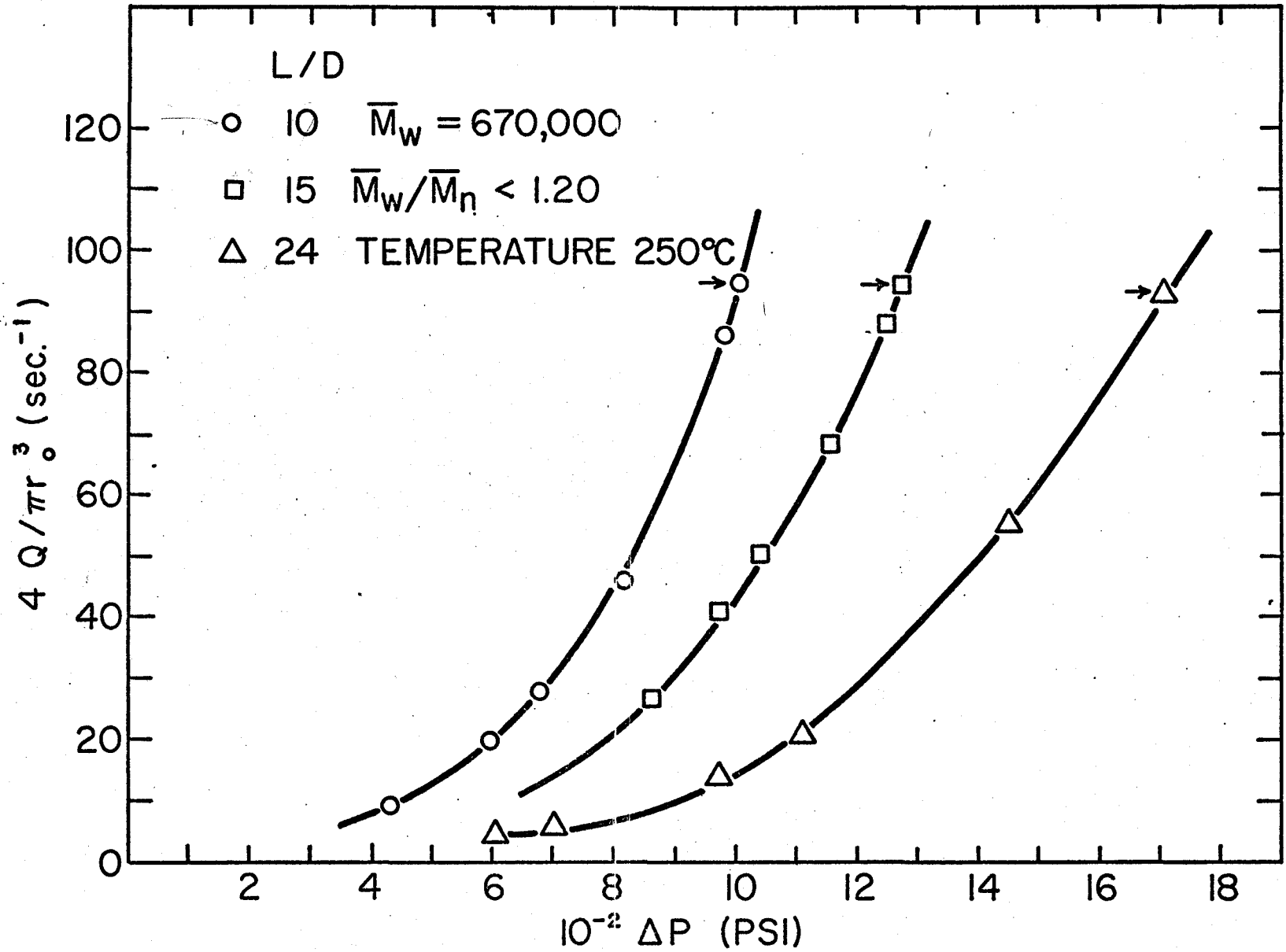


FIG. 9. FLOW CURVES FOR POLYSTYRENE.

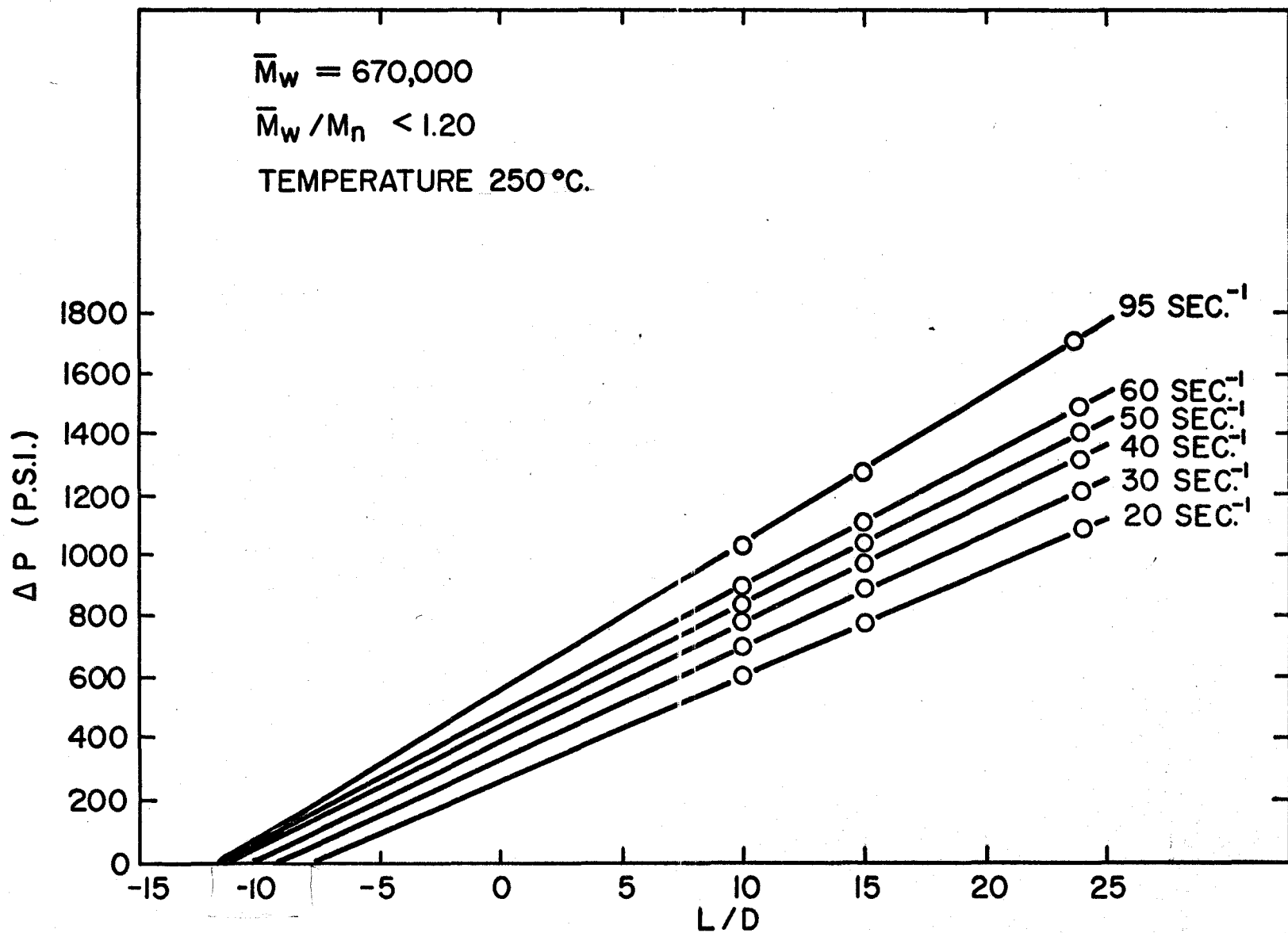


FIG.10. CURVES OF PRESSURE VERSUS L/D. EACH STRAIGHT LINE CORRESPONDS TO A CONSTANT SHEAR RATE.

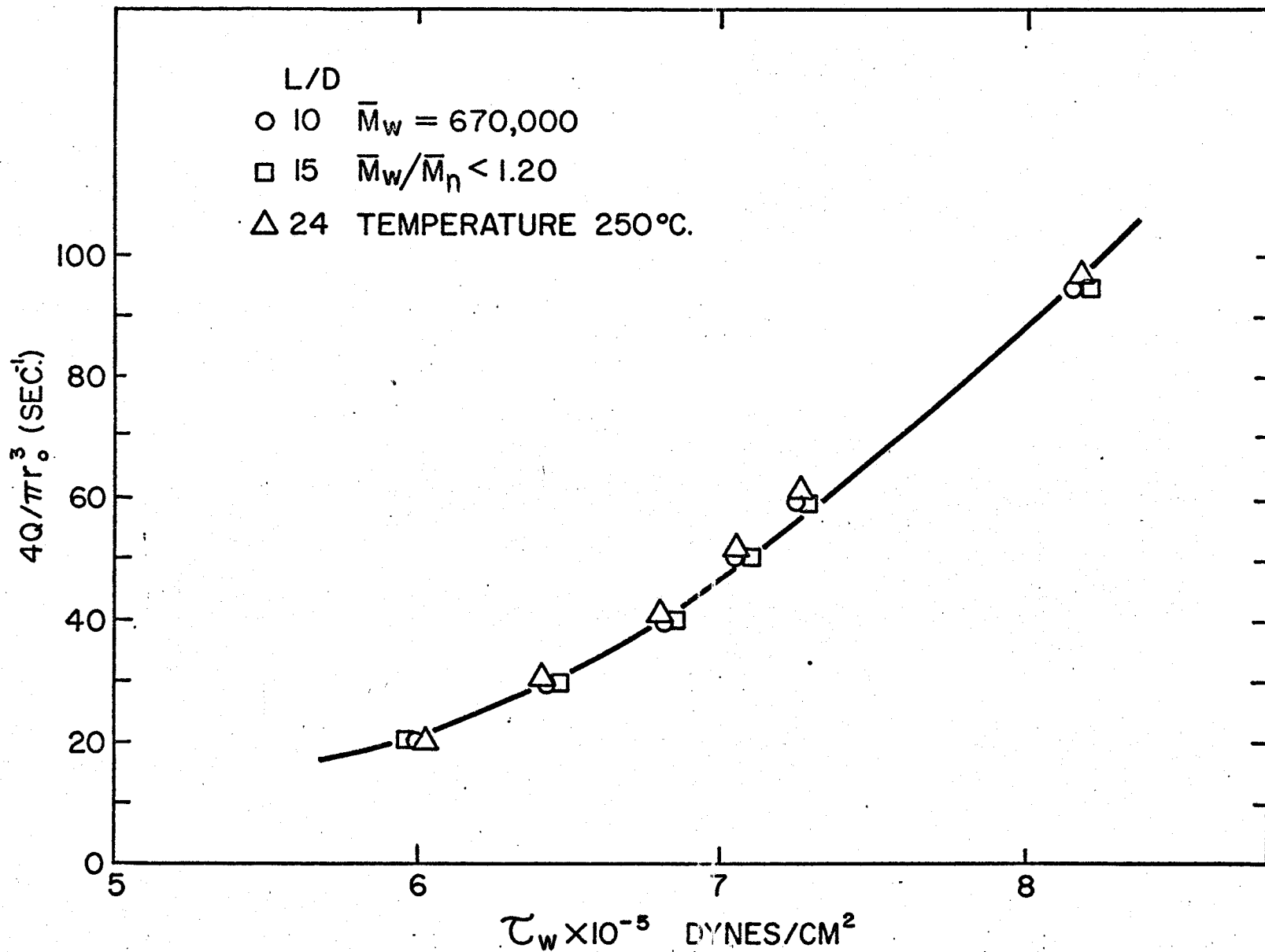


FIG.11. APPARENT SHEAR RATE VERSUS CORRECTED SHEAR STRESS.

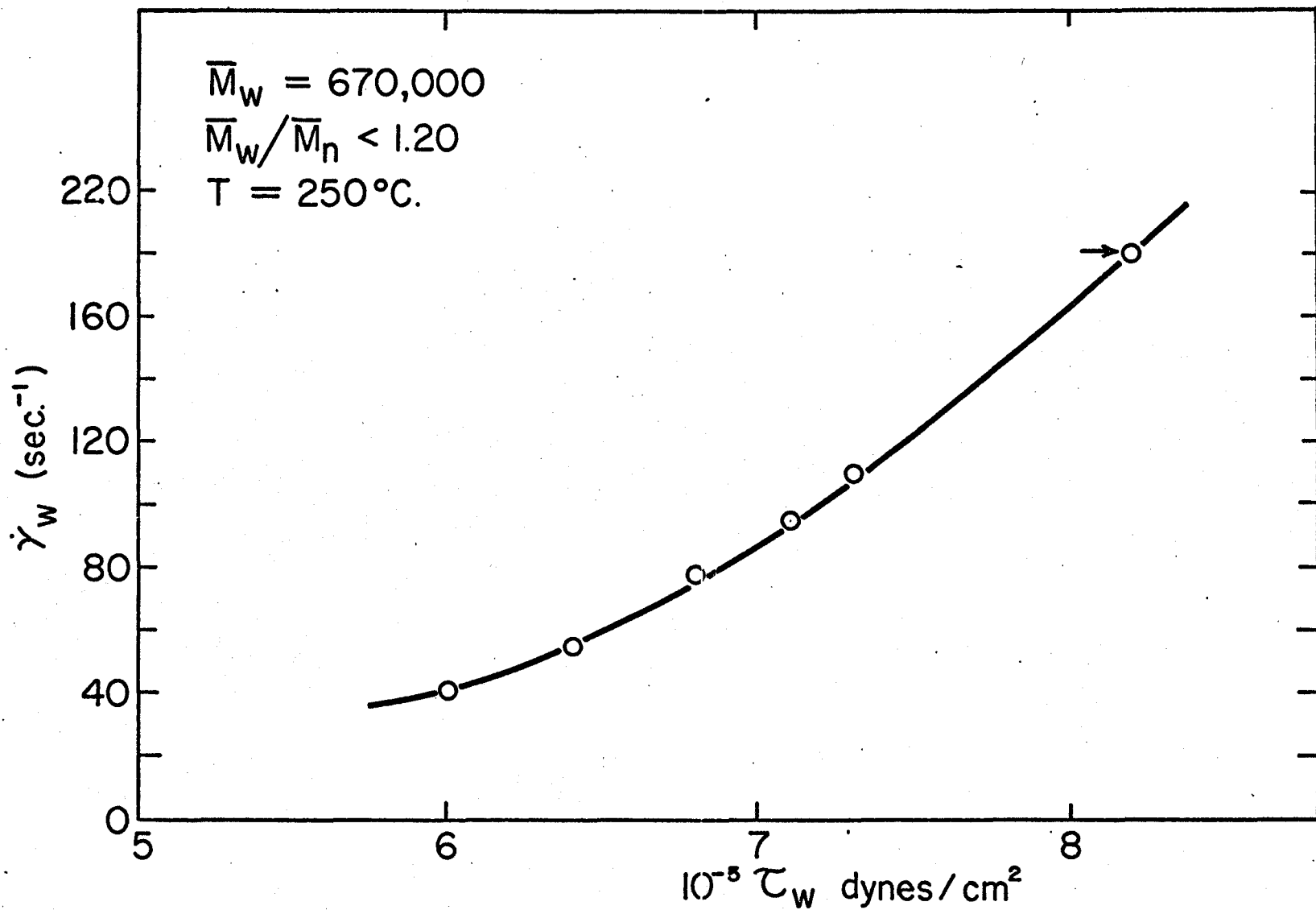


FIG.12 . CORRECTED FLOW CURVE FOR POLYSTYRENE .

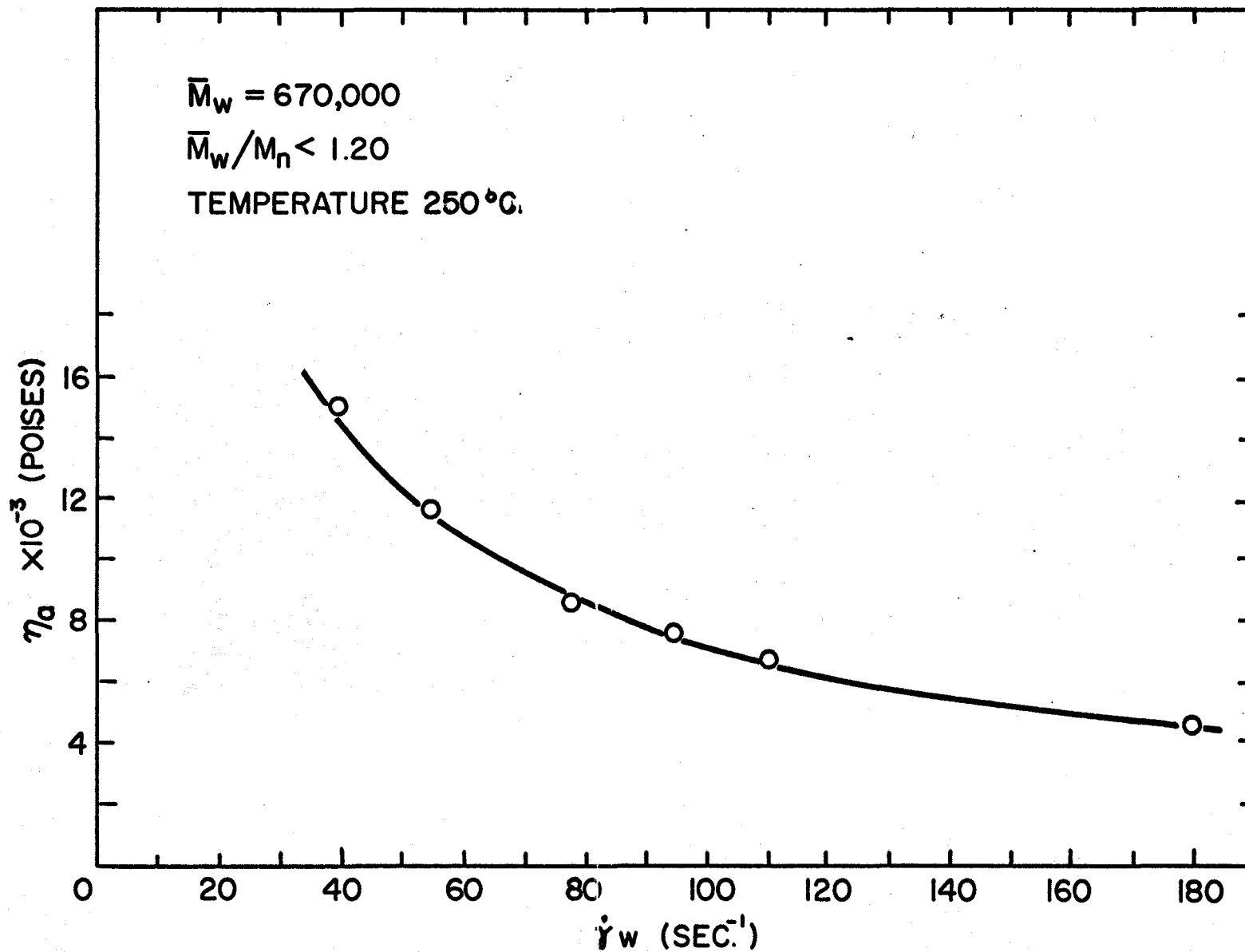


FIG.13. APPARENT VISCOSITY VERSUS SHEAR RATE.

TABLE III CRITICAL CONDITIONS OF POLYSTYRENE

\bar{M}_w	\bar{M}_w/\bar{M}_n	τ_{cr} (dynes/cm ²)	$\dot{\gamma}_{cr}$ (sec ⁻¹)	η_{cr}/η_0	$\tau_{cr} \times \bar{M}_w$	Temperature °C
97,200	<1.06	1.92×10^6	--	--	1.88×10^{11}	158
97,200	<1.06	2.15×10^6	--	--	2.08×10^{11}	170
128,000	2.9	1.6×10^6	--	--	2.05×10^{11}	170
200,000	<1.06	1.37×10^6	105	0.0076	2.76×10^{11}	170
200,000	<1.06	1.34×10^6	--	--	2.68×10^{11}	194
204,450	6.9	1.36×10^6	--	--	2.78×10^{11}	180
207,250	9.21	1.3×10^6	--	--	2.69×10^{11}	180
207,300	2.78	1.17×10^6	--	--	2.42×10^{11}	170
212,000	2.71	1.4×10^6	182	0.0035	2.97×10^{11}	170
355,000	2.92	1.03×10^6	27	0.0034	3.66×10^{11}	170
355,000	2.92	1.06×10^6	1,090	0.0022	3.76×10^{11}	210
355,000	2.92	1.12×10^6	3,000	0.0027	3.98×10^{11}	230
498,000	<1.20	1.17×10^6	4.21	0.055	5.83×10^{11}	194
498,000	<1.20	1.28×10^6	50.0	0.0162	6.37×10^{11}	210
498,000	<1.20	1.30×10^6	135.0	0.0196	6.47×10^{11}	230
600,000	2.32	1.14×10^6	100.0	0.0021	6.85×10^{11}	200
670,000	<1.10	0.73×10^6	30.0	0.022	4.90×10^{11}	230
670,000	<1.10	0.82×10^6	180.0	0.0086	5.5×10^{11}	250
760,000	2.60	0.97×10^6	85.0	0.0007	7.36×10^{11}	200
1,060,000	2.31	1.06×10^6	19.0	0.0012	11.2×10^{11}	200
1,350,000	2.14	0.70×10^6	--	--	9.45×10^{11}	170
1,800,000	<1.20	0.68×10^6	3.6	0.0055	12.2×10^{11}	230
1,800,000	<1.20	0.715×10^6	12.80	0.0034	12.9×10^{11}	250

- terion that $\eta_{cr}/\eta_0 = 0.025$ does not seem to hold.
3. The critical shear stress is practically independent of temperature, within the limits of experimental error. However, some carefully controlled experiments were carried out using the broad distribution sample of $\bar{M}_w = 355,000$. The result is shown in Figure (14). The shear stress at the onset of fracture seems to increase only slightly with temperature.
 4. The influence of polydispersity on critical shear stress is negligible, in full agreement with the results of the bulk of literature (6, 47).

In Figure (15), τ_{cr} (average) is plotted against $1/\bar{M}_w$. It is seen that the results for all the samples are well represented by a single straight line. A least squares fit yielded the expression

$$\tau_{cr} = 0.785 \times 10^6 + 1.14 \times 10^{11} \frac{1}{\bar{M}_w} \quad (6-2)$$

From equation (6-2) one may obtain

$$\tau_{cr} \times \bar{M}_w = 1.14 \times 10^{11} + 0.785 \times 10^6 \times \bar{M}_w \quad (6-3)$$

This is also shown in Figure (16), and it is clearly in contrast with Bagley's (37) conclusion that $\tau_{cr} \times \bar{M}_w = \text{constant}$. However, Bagley's result was supported by Spencer and Dillon's (2) data, who have carried out experiments for a rather limited range of molecular weights (196,000 to 527,000).

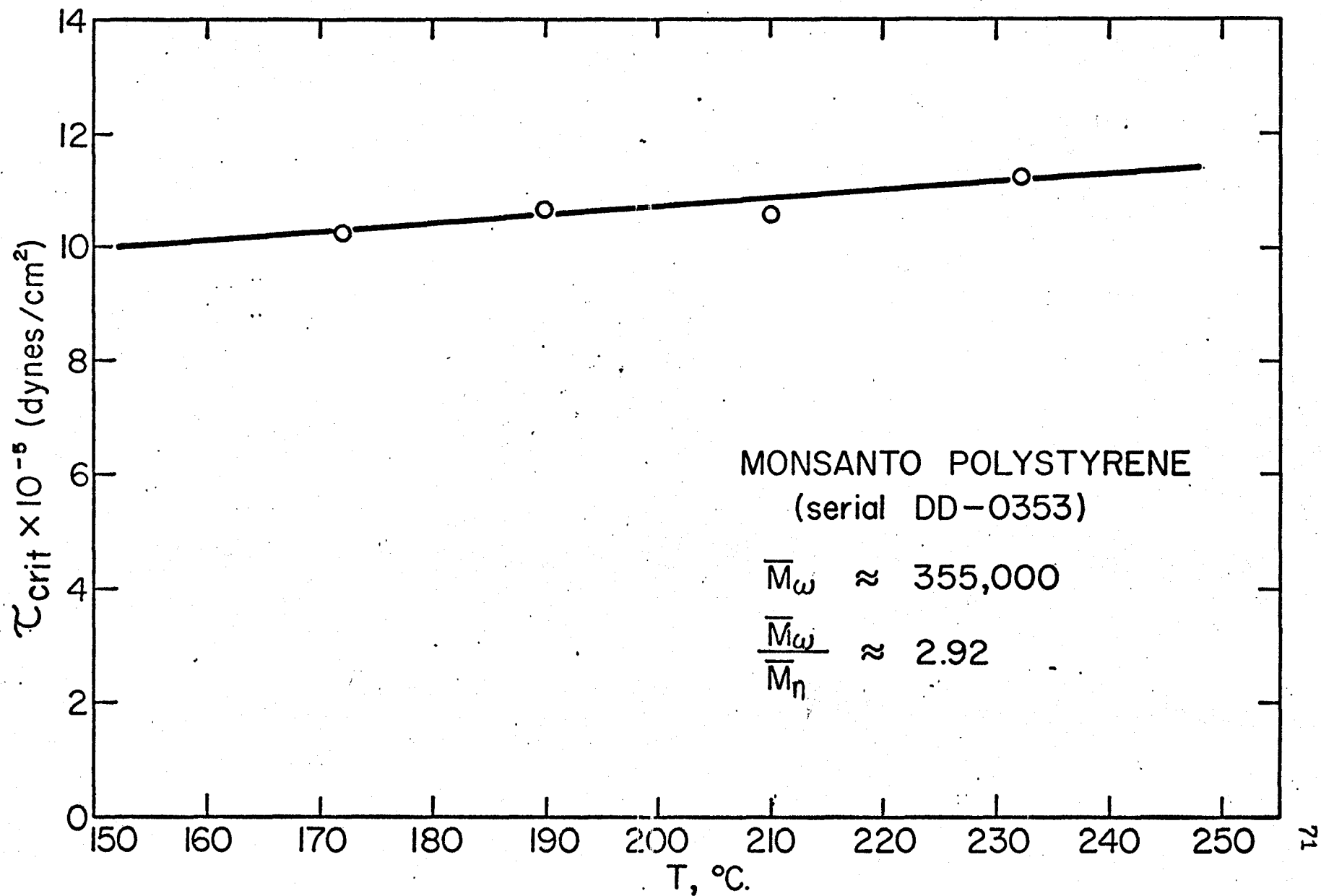


FIG.14. CRITICAL SHEAR STRESS DEPENDENCE ON TEMPERATURE.

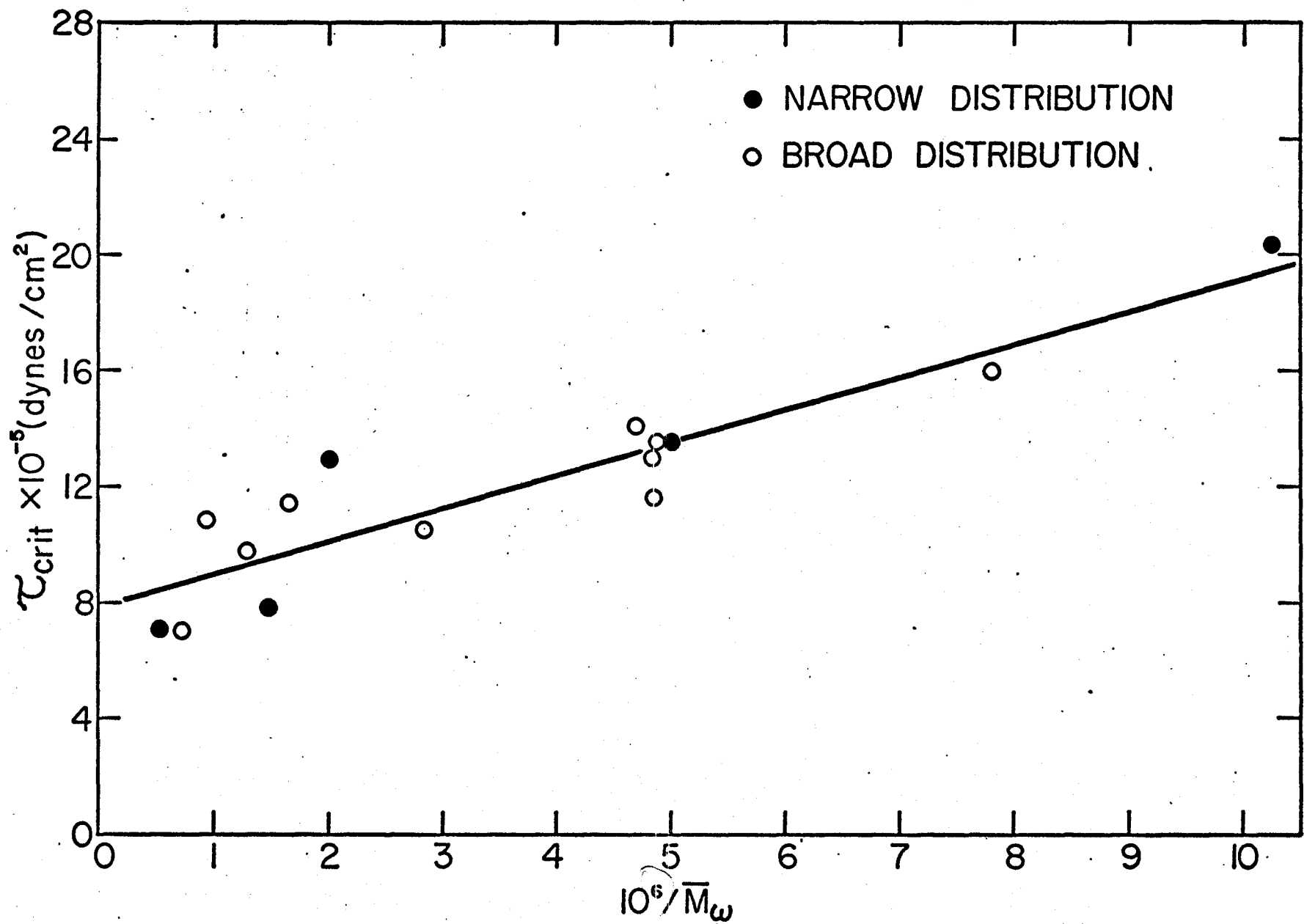


FIG.15.

CRITICAL SHEAR STRESS VS. $1/\bar{M}_w$

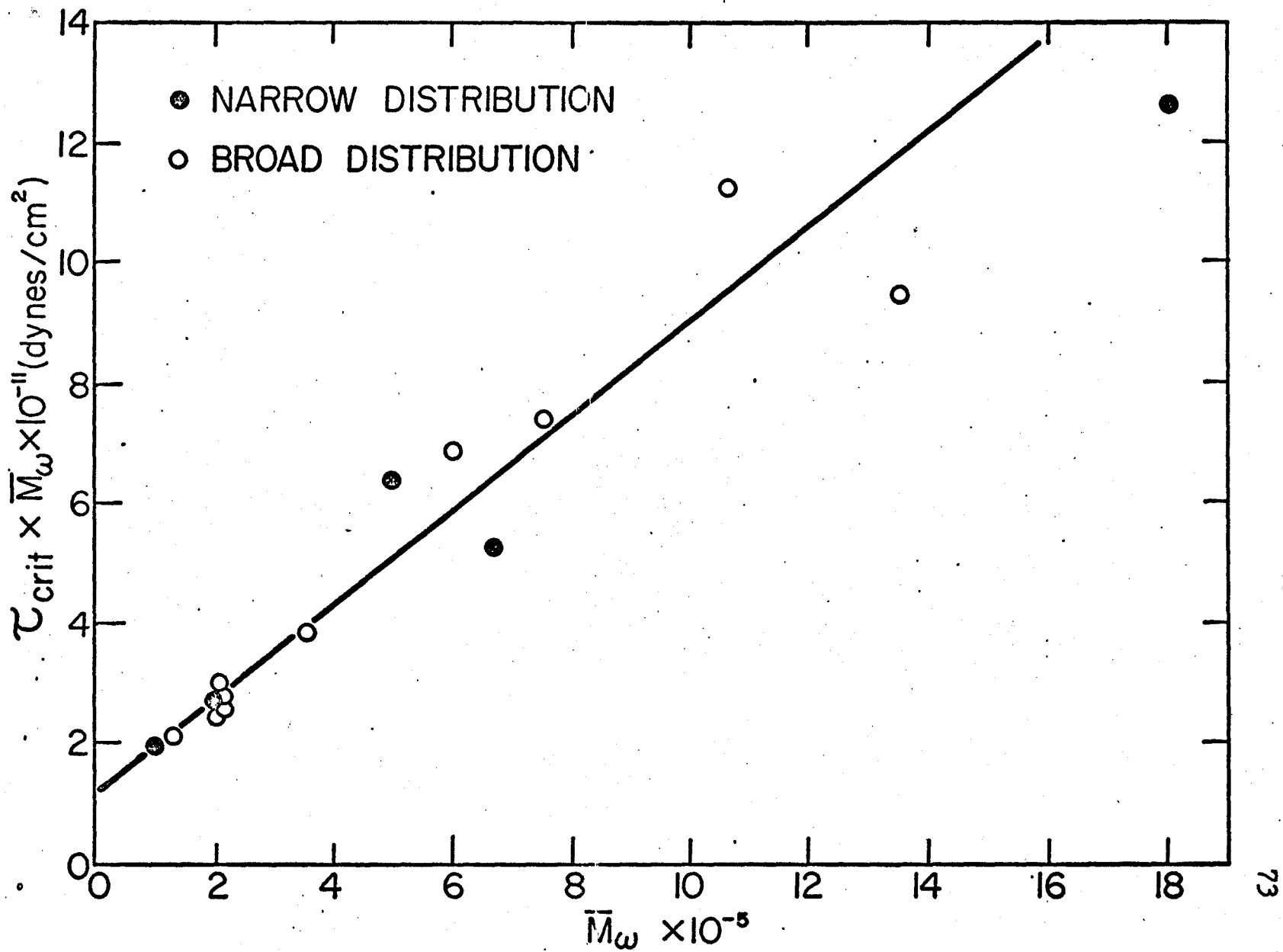


FIG. 16.

DEPENDENCE OF $\tau_{crit} \times \bar{M}_w$ ON \bar{M}_w

It is interesting to note that when τ_{cr} is plotted against $1/\bar{M}_w$ for the present set of data and the data given in References (2, 46), as shown in Figure (17), the discrepancies do not seem really large and may well be attributed to experimental errors. In fact, the straight line which is the least squares fit for our data falls between the data of Spencer and Dillon (2) and Barnett (46). In addition, it must be noted that the experimental range of the present work is extended from $\bar{M}_w = 97,200$ to $\bar{M}_w = 1.8 \times 10^6$ which is a much larger range than in any previous investigation.

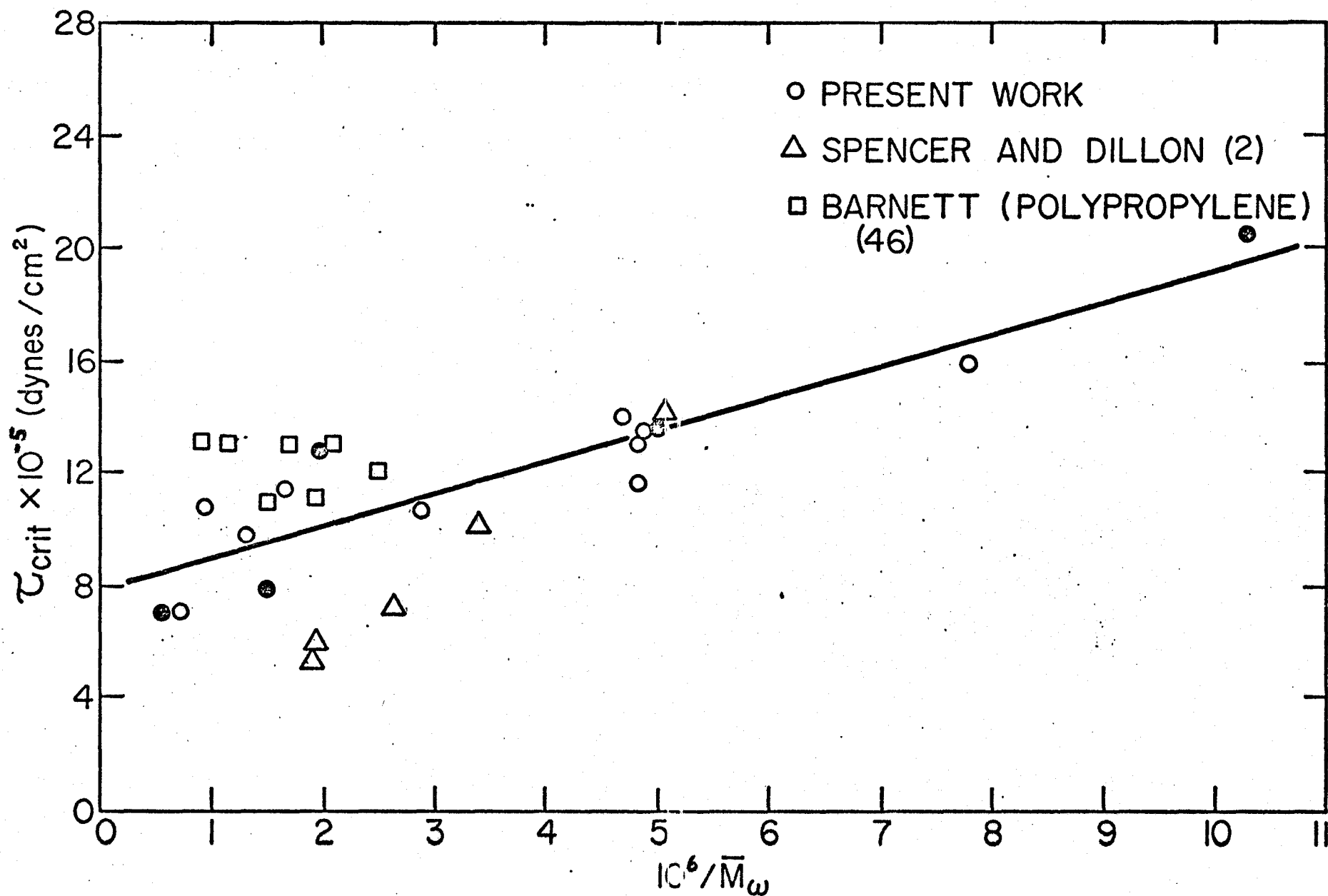


FIG.17. CRITICAL SHEAR STRESS VS. $1/\bar{M}_w$. NARROW DISTRIBUTION SAMPLES ARE REPRESENTED BY CLOSED SYMBOLS.

7. ANALYSIS

Bagley (37, 68) and White (35) conjectured that the onset of melt fracture occurs at constant value of "recoverable shear strain"

$$S_R = \tau_{cr} J \quad (\text{Hooke's law}) \quad (7-1)$$

where J is the steady-state shear compliance. Bagley has taken the value of J as

$$J = \frac{\bar{M}_W}{\rho RT}$$

according to an expression given by Wall (69). White (35) has taken the value of J as the value of the steady state shear compliance of a monodisperse collection of Rouse chains. This value is given by Ferry (70)

$$J_R = \frac{2}{5} \frac{1}{v k_B T}$$

in which v is the number of chains per unit volume, k_B is Boltzmann's constant and T the absolute temperature. For the case in which there are no entanglements

$$v = \frac{\rho N}{\bar{M}_W}$$

so

$$J = \frac{2}{5} \frac{\bar{M}_W}{\rho N k_B T} = \frac{2}{5} \frac{\bar{M}_W}{\rho RT}$$

White has used this expression to prove that

$$\tau_{cr} \times \bar{M}_w = \text{constant}$$

By substituting the value of J into the equation (7-1)

$$S_R = \tau_{cr} \times \frac{2\bar{M}_w}{5\rho RT}$$

and therefore, it follows that

$$\tau_{cr} \times \bar{M}_w = \frac{5}{2} \rho RT S_R = \text{constant}$$

if we suppose that the experimentally observed value of recoverable shear strain is constant.

Recently, it has been shown that the non-Newtonian properties of long-chain polymers are associated with the presence of entanglements (71). According to this theory (71) the entanglements provide a network which is able to store elastic energy, in much the same way as a deformed specimen of cross-linked rubber. Because the recoverable strain represents the amount of elastically stored energy, it is reasonable to associate the phenomenon of melt fracture with the presence of a network due to entanglement (72). According to Graessley's theory (73) there is a characteristic time λ_0 , constant for the polymer, and its magnitude controls the time for formation of molecular chain entanglements between any molecule in the system and other molecules. Its value is of the order of the Rouse relaxation time λ_R where

$$\lambda_R = \frac{6}{\eta^2} \frac{\eta_0 \bar{M}_w}{eRT}$$

Graessley (73) found that the ratio λ_0/λ_R for monodisperse systems is a simple function of molecular weight \bar{M}_w which is:

$$\lambda_0/\lambda_R = \frac{2.00}{1 + 0.17E} \quad (7-2)$$

where $E = \frac{\bar{M}_w}{16,500}$

The same form of variation holds for the relaxation time associated with normal stress. At low shear rates:

$$\tau_{zz} - \tau_{rr} = k_N \dot{\gamma}^2 \quad (7-3)$$

where k_N is the normal stress coefficient.

For a polydisperse collection of Rouse chains we have:

$$k_R = \frac{2\pi^2}{15} \eta_0 \lambda_R \frac{\bar{M}_z \bar{M}_{z+1}}{\bar{M}_w^2} \quad (7-4)$$

Graessley evaluated an experimental time constant λ_N

$$\lambda_N = \frac{15k_N}{\eta_0 \pi^2} \frac{\bar{M}_w^2}{\bar{M}_z \bar{M}_{z+1}} \quad (7-5)$$

where k_N represents the experimental values of normal stress coefficient given by the equation,

$$k_N = \lim_{\gamma \rightarrow 0} \frac{\tau_{zz} - \tau_{rr}}{\gamma^2}$$

The ratios, λ_0/λ_R and λ_N/λ_R measure the deviation of any polymer from the Rouse theory. Graessley found that λ_N/λ_R for monodisperse systems obeys a relation of the form of equation (7-2) which is:

$$\frac{\lambda_N}{\lambda_R} = \frac{2.2}{1 + 0.34E}$$

where $E = \frac{\bar{M}_w}{16,500}$

For the case in which the chains behave like a Rouse chain and there are no entanglement points in each chain, we can combine equation (7-3) with the equation (Reference 35)

$$\tau_{zz} - \tau_{rr} = 2\tau_{zr}S_R$$

to prove that (Appendix II)

$$S_R = \frac{2}{5} \frac{\bar{M}_w \tau_{zr}}{eRT} \quad (\text{White criterion})$$

But in real systems, however, the properties are changed as entanglements are introduced randomly and successively between the chains. Chomppf and Duiser (74) proved that the equilibrium compliance of a cross-linked network of Rouse chains is given by:

$$J = \frac{2}{v_a kT}$$

where v_a is the number of active network elements per unit volume. Graessley (73) shows that:

$$\frac{J_R}{J} = 1 \quad (E \ll 1)$$

$$\frac{J_R}{J} = \frac{1}{5} E \quad (E \gg 1)$$

The first equation gives $J = J_R$ so from equation (7-1) we obtain $\tau_{cr} \times \bar{M}_w = \text{constant}$. The second equation gives $J = \frac{5J_R}{E} = \text{constant}$. This case was supported experimentally lately (75). If we substitute this value into equation (7-1) we obtain $\tau_{cr} = \text{constant}$. This has been observed by Barnett (46) for polypropylene.

On the basis of the previous discussion, it is easy to arrive at the conclusion that neither the $\tau_{cr} \times \bar{M}_w$ nor τ_{cr} are constants because both represent extreme cases. Incipience of fracture however, can take place and at intermediate entanglement densities.

At the limit of zero shear $\frac{J}{J_R} = \frac{\lambda_N}{\lambda_R}$ (as it is shown in Appendix III). So at finite shear rates one might expect

$$\frac{J}{J_R} = \frac{A}{1 + BE} \quad (7-6)$$

The ratio $\frac{J}{J_R}$ represents the deviation in the behaviour of any sample from the Rouse theory.

Then, setting

$$\tau_{cr} \times J = S_R$$

and, for a monodisperse system

$$J_R = \frac{2}{5} \frac{\bar{M}_W}{\rho RT}$$

one obtains a linear relationship between $\tau_{cr} \times \bar{M}_W$ and \bar{M}_W , that is,

$$\tau_{cr} \times \bar{M}_W = \frac{5}{2} \frac{\rho R S_R T}{A} \left(1 + \frac{B}{16,500} \bar{M}_W \right) \quad (7-7)$$

which is of the same form as equation (6-3) obtained by a least squares fit of the experimental data.

For a polydisperse system, House's expression is (70):

$$J_R = \frac{2}{5} \frac{\bar{M}_W}{\rho RT} \left(\frac{\bar{M}_z \bar{M}_{z+1}}{\bar{M}_W^2} \right)$$

in which the factor $\bar{M}_z \bar{M}_{z+1} / \bar{M}_W^2$ implies a large dependence on the molecular weight distribution, especially in the high molecular weight tail. The fact, however, that the same type of equation is obeyed by both narrow and broad molecular weight distribution samples suggests that \bar{M}_W rather than $\bar{M}_W \left(\frac{\bar{M}_z \bar{M}_{z+1}}{\bar{M}_W^2} \right)$ should be used in J_R when Graessley's expression for J/J_R is applied, which also has \bar{M}_W as the correlating variable.

By comparing with equation (6-3) which is a least squares fit of the experimental data we obtain

$$A = \frac{S_R}{1.16} \quad (7-8)$$

$$B = 0.113 \quad (7-9)$$

The values of A, and B were calculated by taking an average temperature $T = 473^\circ\text{K}$. Graessley's constants were $A = 2.2$ and $B = 0.34$ respectively at the limit of zero shear.

At finite shear rates one might assume

$$\frac{J}{J_R} = \frac{A}{1 + k_2 \left(\frac{E}{E_0} \right) E_0} \quad (7-10)$$

Then

$$B = k_2 \frac{E}{E_0}$$

where E_0 is the entanglement density at $\dot{\gamma} = 0$ and E is the entanglement density at finite shear rates. The ratio $E/E_0 = g(\dot{\gamma})$ is the entanglement density ratio given by Graessley's entanglement theory (76).

Setting Graessley's value for $k_2 = 0.34$, one obtains $E_{cr}/E_0 = 0.332$, which means that melt fracture occurs at sufficiently high shear rates when the entanglement density is reduced to one third of its value at zero shear. Therefore, melt fracture is due to the relatively large loss of entanglement points. It is interesting to note that this result is related to Bartos' criterion that melt fracture occurs at

$\frac{\eta_{cr}}{\eta_0} = 0.025$. Graessley (73) gives $E/E_0 = 0.486$ for $\frac{\eta}{\eta_0} = 0.0302$ and $E/E_0 = 0.415$ for $\frac{\eta}{\eta_0} = 0.0148$. The large range of values of $\frac{\eta_{cr}}{\eta_0}$ shown in Table III is probably due to the fact that small changes in E/E_0 correspond to large differences in $\frac{\eta}{\eta_0}$, which was also pointed out by Malkin and Vinogradov (77) in a similar way. Moreover, the equation (6-1) which was used for the calculation of η_0 is not always accurate.

In Graessley's paper (73) an experimentally determined constant $A = 2.2$ is given and therefore, using $S_R = A \times 1.16$ one obtains $S_R = 2.56$. This means that fracture occurs at a value of a recoverable shear strain of 2.56 units. This is different from Bagley's result ($S_R \approx 7.0$) because of the factor $2/5$ used in the expression for J_R .

In Figure 18, τ_{cr}/T vs. $1/\bar{M}_w$ is plotted and the solid line through the points is the least squares fit

$$\frac{\tau_{cr}}{T} = 0.152 \times 10^4 + 2.965 \times 10^8 \frac{1}{\bar{M}_w}$$

A comparison with equation (7-7) yields

$$A = \frac{S_R}{1.42} \quad \text{and} \quad B = 0.0845$$

Therefore for $A = 2.2$ and $k_2 = 0.34$ we obtain $E_{cr}/E_0 = 0.254$ and $S_R = 3.12$.

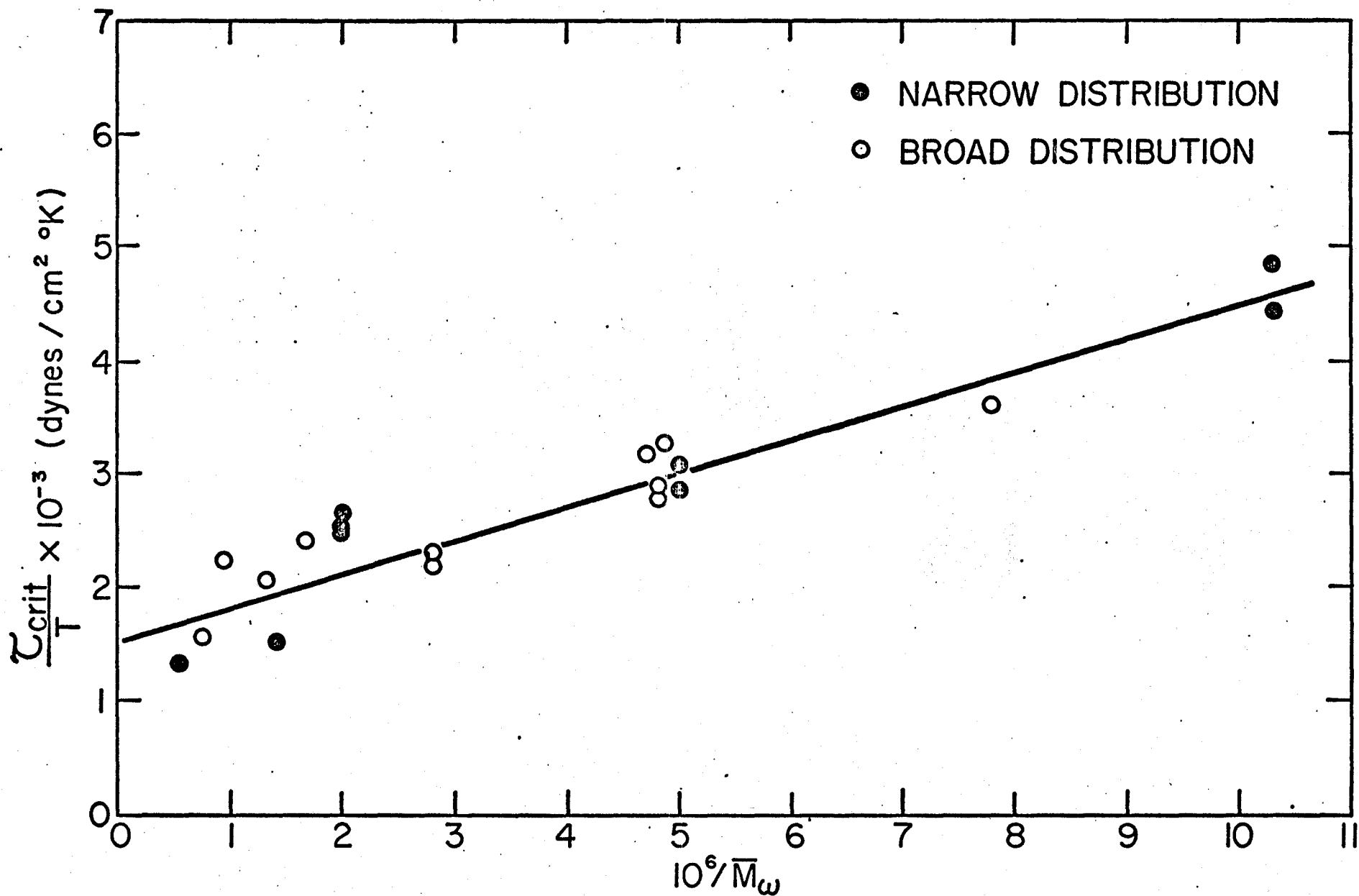


FIG.18.

CRITICAL SHEAR STRESS FROM ENTANGLEMENT THEORY VS. $1/\bar{M}_w$.

8. CONCLUSIONS

1. The melt fracture is ultimately molecular in nature and seems logical to correspond to the breakdown of the molecular entanglement network.
2. The critical shear stress is a linear function of $1/M_w$.
3. The critical shear stress increases slightly with temperature.
4. The critical shear stress is independent of polydispersity.
5. The behaviour of polystyrene at the onset of melt fracture can be well described using Hooke's law for constant recoverable shear strain and the results of Graessley's entanglement theory.

9. NOMENCLATURE

A	constant
b	compressibility of the fluid
B	constant
C_v	heat capacity at constant volume
D	capillary diameter
D_s	diameter of the emerging polymer from the capillary
E	entanglement density at finite shear rates
E_0	entanglement density at zero shear rates
E_{cr}	entanglement density at incipience of melt fracture
$f(M)$	molecular weight distribution function
F	force tangentially applied to a flowing surface
g_r	r-component of the gravity vector
g_z	z-component of the gravity vector
g_θ	θ -component of the gravity vector
J	shear compliance
J_R	Rouse's shear compliance
k	coefficient of thermal expansion
k_B	Boltzmann's constant
k_N	normal stress coefficient
k_0	power law constant
k_R	normal stress coefficient for a polydispersed collection of Rouse chains
k_2	constant
K	thermal conductivity

L	tube length
L_e	entrance length
L_s	length of the steady state region
\bar{M}_n	number average molecular weight
\bar{M}_w	weight average molecular weight
\bar{M}_z	z-average molecular weight
\bar{M}_{z+1}	z+1-average molecular weight
n	power law constant
N	Avogadro's number
P_0	ambient pressure
Pe'	Peclet number
$P_{rr}, P_{zz}, P_{\theta\theta}$	normal stresses
P_s	pressure gradient
\bar{q}	heat flux vector
Q	volumetric flow rate
r, θ, z	cylindrical coordinates
r_0	capillary radius
R	ideal gas constant
Re	Reynolds number
S	surface
S_R	recoverable shear strain
T	temperature
T_0	reservoir temperature
V	volume
\bar{V}	velocity vector
V_m	average velocity

V_r, V_θ, V_z	scalar components of V in cylindrical coordinates
V_s	slip velocity
w_i	weight fraction of the i -th component
Z	number of monomer units in the polymer chain
Z_0	dimensionless length

Greek letters

$\dot{\gamma}$	shear rate
$\dot{\gamma}_{cr}$	critical shear rate
$\dot{\gamma}_w$	shear rate at the wall
η	viscosity
η_a	true apparent viscosity
η_{ap}	apparent viscosity
η_{cr}	critical viscosity
η_0	zero shear viscosity
θ_0	dimensionless temperature
λ_0	viscosity relaxation time
λ_N	relaxation time associated with normal stress
λ_R	Rouse relaxation time
μ	Newtonian viscosity
ν	number of polymer chains per unit volume
ν_a	number of active network elements per unit volume
ζ	Oldroyd's parameter
ρ	density
σ_1, σ_2	normal stress coefficients
τ	shear stress

$\bar{\tau}$	shear stress tensor
τ_{ap}	apparent shear stress
τ_{cr}	critical shear stress
$\tau_{rr}, \tau_{\theta\theta}, \tau_{zz},$ $\tau_{r\theta}, \tau_{rz}, \tau_{\theta z}$	scalar components of $\bar{\tau}$ in cylindrical coordinates
τ_w	shear stress at the wall
ϕ	Oldroyd's parameter

Mathematical Symbols

∇	"del" vector operator
$\frac{D}{Dt}$	substantive derivative
$\frac{\partial}{\partial t}, \frac{\partial}{\partial r}, \frac{\partial}{\partial \theta}, \frac{\partial}{\partial z}$	partial derivatives
Σ	summation

REFERENCES

- 1 NASON, H.K. J. Appl. Phys. 16, 338 (1945).
- 2 SPENCER, R.S. and R.E. DILLON. J. Colloid. Sci. 4, 241 (1949).
- 3 TORDELLA, J.P. J. Appl. Physics, 27, 454 (1956).
- 4 McKELVEY, J.M. "Polymer Processing", John Wiley and Sons, Inc., New York, 1962.
- 5 MIDDLEMAN, S. and J. GAVIS. Physics of Fluids, 4, 355 (1961).
- 6 HOWELLS, E.R. and J.R. BENBOW. Trans. J. Plastics Inst. 30, 240 (1962).
- 7 CLEGG, P.L. Trans. J. Plastics Inst. 28, 245 (1960).
- 8 KENDALL, V.C. Trans. J. Plastics Inst. 31, 49 (1963).
- 9 HUCK, N.D. and P.L. Clegg. S.P.E. Trans. 1, 121 (1961)
- 10 DENNISON, M.T. Trans. J. Plastics Inst. 35, 803 (1967).
- 11 TORDELLA, J.P. "Rheology" (ed. F.R. Firich), Vol.5 (to be published), Academic Press.
- 12 WESTOVER, R.F. and B. Maxwell. S.P.E.J. 13, 27 (1957).
- 13 TORDELLA, J.P. Rheol. Acta, 213, 216 (1958).
- 14 METZNER, A.B. and J.C. REED. A.I.Ch.E.J. 1, 434 (1955).
- 15 BIRD, R.B. S.P.E.J. 11, 35 (1955).
- 16 COLWELL, R.E. S.P.E.J. 11, 24 (1955).
- 17 MARTIN, B. Int. J. Non-Linear Mech. 2, 285 (1967).
- 18 LYPTON, J.M. and J.L. REGESTER. Polymer Eng. Sci. 5, 235 (1965).
- 19 POLLET, W.F. Brit.J.Appl.Phys. 6, 199 (1955).
- 20 VINOGRADOV, G.V. and I.M. BALKIN. J. Polymer Sci. Part A, 3, 917 (1965).

- 21 TORDELLA, J.P. S.P.E.J. 12, 36 (1956).
- 22 TORDELLA, J.P. Trans. Soc. Rheology, 1, 203 (1957).
- 23 TORDELLA, J.P. S.P.E.J. 13, 36 (1957).
- 24 METZNER, A.B., E.L. CARLEY, and I.K. PARK. Modern Plastics, 37, 133 (1960).
- 25 BEYNON, D.L. and B.J. GLYDE. British Plastics, 33, 414 (1960).
- 26 BAGLEY, E.B. and A.M. BIRKS. J. Appl. Phys. 31, 556 (1960).
- 27 MILLS, D.R., G.E. MOORE, and D.W. RIGH. S.P.E.Trans. 1, 40 (1961).
- 28 SCHULKEN, R.M. and R.E. BOY. S.P.E.J. 16, 423 (1960).
- 29 REINER, M. "Deformation, Strain and Flow" (H.K. Lewis and Co., London, 1949).
- 30 BENBOW, J.J. and P. LAMB. S.P.E.Trans. 3, 7 (1963).
- 31 KENNAWAY, A. "Plastics Progress" (Icliffe, London, 1957) pp. 149.
- 32 GALT, J. and B. Maxwell. Modern Plastics, 42, 115 (1964).
- 33 MAXWELL, B. and J. GALT. J. Polymer Sci. 62, 553 (1962).
- 34 WESTOVER, R.F. Polymer Eng. Sci. 6, 83 (1966).
- 35 WHITE, J.L. J. Appl. Poly. Sci. 8, 2339 (1964).
- 36 METZNER, A.B., J.L. White, and M.M. Denn. A.I.Ch.E.J. 12, 863 (1966).
- 37 BAGLEY, E.B. Trans. Soc. Rheol. 5, 355 (1961).
- 38 PHILIPPOFF, W. and F.H. GASKINS. Trans. Soc. Rheol. 2, 263 (1958).
- 39 TORDELLA, J.P. J. Appl. Polymer Sci. 7, 215 (1963).
- 40 MENEFEY, E. J. Appl. Polymer Sci. 8, 849 (1964).

- 41 METZGER, A.P., C.W. HAMILTON, and E.H. MERZ. S.P.E.Trans. 3,
21 (1963).
- 42 HAMMOND, L.R. Wire and Wire Products, 35, 725 (1960).
- 43 FERRARI, A.G. Wire and Wire Products, 39, 1036 (1964).
- 44 CLEGG, P.L. "Rheology of Elastomers" (Pergamon Press,
Oxford, 1957)pp.174.
- 45 SIEGLAFF, C.L. S.P.E.Trans. 4, 129 (1964).
- 46 BARNETT, S.M. Polymer Eng. and Sci. 7, 168 (1967).
- 47 FERGUSON, J., B. WRIGHT, and R.N. HOWARD. J. Appl. Chem. 14,
53 (1964).
- 48 RABINOWITSCH, B. Z. Physik Chem. (Leipzig) 145, 1 (1929). *OR*
- 49 OLDROYD, J.G. Rheology (ed. F.R. Eirich) Vol.I, Chap.16,
Academic Press.
- 50 BAGLEY, E.B. J. Appl. Phys. 28, 624 (1957).
- 51 TOOR, H.L. Trans. Soc. Rheol. 1, 177 (1957).
- 52 SIEGEL, R.E., M. SPARROW and T.M. HALLMAN. Appl. Sci. Res.
A7, 386 (1958).
- 53 BRINKMAN, H.C. Appl. Sci. Res. A2, 120 (1951).
- 54 MIDDLEMAN, S. "The Flow of High Polymers" (J. Wiley and
Sons, Inc. New York, 1968).
- 55 GERRARD, J.E., F.F. STEIDLER and J.K. APPELDOORN. Ind. Eng.
Chem. Fundamentals, 5, 260 (1966).
- 56 SPENIER, R.S., G.D. GILMORE. J. Appl. Phys. 20, 502 (1949).
- 57 BRODKEY, R.S. "The Phenomena of Fluid Motions" (Addison-
Wesley Publishing Co., 1967).

- 58 GAVIS, J. and S. MIDDLEMAN. J. Appl. Polymer Sci. 7, 493-506, (1963).
- 59 SAVINS, J.G. J. Appl. Polymer Sci. 6, 567 (1962).
- 60 WHITE, J.L. A.I.Ch.E.J. 9, 559-561 (1963).
- 61 GASKINS, H.F. and W. PHILIPPOFF. Trans. Soc. Rheology, 3, 181 (1959).
- 62 GASKINS, H.F. and W. PHILIPPOFF. J. Appl. Polymer Sci. 2, 143 (1959).
- 63 SAKIADIS, B.C. A.I.Ch.E.J. 8, 317 (1962).
- 64 METZNER, A.B., T.W. HOUGHTON, A.R. SAILOR, and J.L. WHITE. Trans. Soc. Rheol. 5, 133 (1961).
- 65 TRUESDELL, C. Trans. Soc. Rheol. 4, 9 (1960).
- 66 NIELSON, L.E. "Mechanical Properties of Polymers" (Rheinhold, 1962) p.58.
- 67 BARTOS, O. J. Appl. Phys. 35, 2767 (1964).
- 68 BAGLEY, E.B. J. Appl. Phys. 31, 1126 (1960).
- 69 WALL, F.T. J. Chem. Phys. 19, 485 (1942).
- 70 FERRY, J.D. "Viscoelastic Properties of Polymers" (John Wiley and Sons, Inc., New York, 1961) pp.169.
- 71 GRAESSLEY, W.C. J. Chem. Phys. 43, 2696 (1965).
- 72 VLACHOPOULOS J. and LIDORIKIS, S. Polymer Eng. and Sci.
(to be published).
- 73 GRAESSLEY, W.C. and L. Segal. Macromolecules, 2, 49 (1969).
- 74 CHOMPFF, A.S. and J.A. DUISER. J. Chem. Phys. 45, 1505 (1966).
- 75 OUOGI, S., T. MASUBA, and K. KITAYANA. Macromolecules, 3, No.2, 109 (1970).

76 GRAESSLEY, W.C. J. Chem. Phys. 47, 1942 (1967).

77 MALKIN, A. and VINOGRADOV, G.V. J. Appl. Poly. Sci. 10,
767 (1966).

APPENDICES

Table I-1

Polystyrene

$$\bar{M}_w = 200,000$$

$$\bar{M}_w/\bar{M}_n = <1.06$$

Temperature: 170°C

L/D	ΔP (psi)	$\tau_{ap} \times 10^{-5}$ dynes/cm ²	$4Q/\pi r_o^3$ (sec ⁻¹)	$\tau_w \times 10^{-5}$ dynes/cm ²	$\dot{\gamma}_w$ (sec ⁻¹)	D_s/D	Remarks
10	1,600	27.50	76.0	13.60	105.00		Fracture
15	1,135 1,470 1,790 2,000	13.00 16.90 20.60 23.00	7.8 26.80 57.50 75.50	9.90 13.20 14.00 13.80	10.00 34.80 79.00 105.0		Fracture
24	1,265 1,600 1,880 2,300 2,710	9.10 11.50 13.50 16.60 19.50	2.26 7.20 16.30 40.7 75.70	7.35 9.75 11.10 13.00 13.70	3.00 9.60 21.80 56.00 105.00		Fracture

$$\tau_{cr} = 13.7 \times 10^5$$

$$\tau_{cr} \times M_w = 2.76 \times 10^{11}$$

Table I-2

Polystyrene

$$\bar{M}_w = 212,000$$

$$\bar{M}_w/\bar{M}_n = 2.71$$

Temperature: 170°C

L/D	ΔP (psi)	$\tau_{ap} \times 10^{-5}$ dynes/cm ²	$4Q/\pi r_o^3$ (sec ⁻¹)	$\tau_w \times 10^{-5}$ dynes/cm ²	$\dot{\gamma}_w$ (sec ⁻¹)	D_s/D	Remarks
10	600	10.30	20	8.75	26.0	1.78	
	840	14.40	35	10.15	46.50	1.80	
	1,000	17.20	48	11.45	64.00	2.06	
	1,220	21.00	70	12.35	96.00	2.26	
	1,420	24.40	99	13.55	135.0	2.33	
	1,580	27.20	130	14.00	182.00	2.47	Fracture
15	600	6.90	15	6.45	19.50	1.80	
	800	9.20	21	8.30	28.00	1.86	
	1,020	11.70	30	9.50	40.50	2.06	
	1,700	19.50	85	13.00	110.00	2.30	
	1,880	21.60	112	13.80	150.00	2.36	
	1,950	22.40	128	14.00	182.00	2.40	Fracture
19.5	540	4.78	10	4.52	13.50	1.75	
	960	8.50	18	7.25	23.80	2.00	
	1,540	13.60	42	10.90	57.00	2.20	
	2,020	17.90	77	13.00	105.00	2.35	
	2,260	20.00	110	13.90	149.0	2.42	
	2,380	21.00	127	14.05	182.00	2.50	Fracture

$$\tau_{cr} = 14 \times 10^5$$

$$\tau_{cr} \times \bar{M}_w = 2.97 \times 10^{11}$$

Table I-3

Polystyrene

$$\bar{M}_w = 355,000$$

$$\bar{M}_w/\bar{M}_n = 2.92$$

Temperature: 170°C

L/D	ΔP (psi)	$\tau_{ap} \times 10^{-5}$ dynes/cm ²	$4Q/\pi r_o^3$ (sec ⁻¹)	$\tau_w \times 10^{-5}$ dynes/cm ²	$\dot{\gamma}_w$ (sec ⁻¹)	D_s/D	Remarks
10	316	5.45	1.6	5.30	2.10		Fracture
	407	6.95	2.0	5.8	2.90		
	600	10.3	3.8	6.7	4.30		
	805	13.9	8.50	8.15	11.20		
	928	16.0	12.40	8.80	14.00		
	1,060	18.2	19.00	10.00	27.00		
15	635	7.30	3.50	6.60	8.00		Fracture
	794	9.15	6.10	7.70	10.20		
	927	10.70	8.50	8.20	10.80		
	1,025	11.80	11.50	8.60	11.40		
	1,240	14.30	17.50	9.30	13.00		
	1,312	15.20	20.00	10.50	27.00		
24	805	5.75	1.36	5.20	6.30		Fracture
	927	6.63	2.72	6.15	7.20		
	1,240	8.85	7.00	7.90	9.50		
	1,670	11.90	16.30	9.30	14.00		
	1,880	13.40	19.50	10.40	27.00		

$$\tau_{cr} = 10.3 \times 10^5$$

$$\tau_{cr} \times \bar{M}_w = 3.66 \times 10^{11}$$

Table I-4

Polystyrene

$$\bar{M}_w = 355,000$$

$$\bar{M}_w/\bar{M}_n = 2.92$$

Temperature: 230°C

L/D	ΔP (psi)	$\tau_{ap} \times 10^{-5}$ dynes/cm ²	$4Q/\pi r_o^3$ (sec ⁻¹)	$\tau_w \times 10^{-5}$ dynes/cm ²	$\dot{\gamma}_w$ (sec ⁻¹)	D_s/D	Remarks
10	180	3.10	15.5	4.20	22.00	—	Fracture
	280	4.8	48.3	5.30	62.00	—	
	405	6.95	154	6.40	220.00	—	
	630	10.80	535	7.50	705.00	—	
	780	13.40	952	8.40	1,500	—	
	930	16.00	1,875	11.2	3,000	—	
15	430	4.95	37.2	4.83	48.00	—	Fracture
	550	6.33	89.0	6.8	130.00	—	
	800	9.20	340	7.65	490.00	—	
	1,030	11.80	825	8.5	1,200	—	
	1,200	13.80	1,370	9.35	2,100	—	
	1,320	15.20	1,870	11.3	3,000	—	
24	510	3.70	30.2	3.2	42.00	—	Fracture
	800	5.73	105	5.5	135.00	—	
	1,210	8.65	370	7.9	502.00	—	
	1,430	10.20	725	8.95	1,020.00	—	
	1,630	11.60	1,180	9.15	1,680	—	
	1,820	13.00	1,890	11.2	3,000	—	

$$\tau_{cr} = 11.2 \times 10^5$$

$$\tau_{cr} \times M_w = 3.98 \times 10^{11}$$

Table I-5

Polystyrene

$$\bar{M}_w = 498,000$$

$$\bar{M}_w/\bar{M}_n = <1.20$$

Temperature: 194°C

L/D	ΔP (psi)	$\tau_{ap} \times 10^{-5}$ dynes/cm ²	$4Q/\eta r_o^3$ (sec ⁻¹)	$\tau_w \times 10^{-5}$ dynes/cm ²	$\dot{\gamma}_w$ (sec ⁻¹)	D_s/D	Remarks
10	384	6.60	0.20	6.05	0.25	1.0	Fracture
	475	8.15	0.475	7.80	0.65	1.03	
	605	10.40	1.00	9.45	1.30	1.05	
	770	13.25	2.01	10.30	2.70	1.10	
	850	14.60	3.00	11.70	4.21	1.17	
15	535	6.15	0.25	5.90	0.30	1.06	Fracture
	605	6.95	0.36	6.85	0.49	1.07	
	700	8.05	0.58	7.75	0.79	1.09	
	870	10.00	1.15	9.30	1.55	1.16	
	1,086	12.50	2.20	10.90	2.94	1.27	
	1,200	13.80	2.95	11.65	4.21	1.27	
24							

$$\tau_{cr} = 11.7 \times 10^5$$

$$\tau_{cr} \times M_w = 5.83 \times 10^{11}$$

Table I-6

Polystyrene

$$\bar{M}_w = 498,000$$

$$\bar{M}_w/\bar{M}_n = <1.20$$

Temperature: 210°C

L/D	ΔP (psi)	$\tau_{ap} \times 10^{-5}$ dynes/cm ²	$4Q/\pi r_o^3$ (sec ⁻¹)	$\tau_w \times 10^{-5}$ dynes/cm ²	$\dot{\gamma}_w$ (sec ⁻¹)	D_s/D	Remarks
10	362	6.24	1.50	6.12	1.90	1.00	
	496	8.55	4.00	8.30	5.40	1.09	
	600	10.30	7.70	10.00	10.00	1.15	
	724	12.50	13.70	11.70	18.50	1.17	
	850	14.60	24.20	12.10	33.00	1.20	
	925	15.90	37.00	12.80	50.00	1.23	
15	475	5.45	0.40	5.40	0.52	1.10	
	543	6.25	0.60	6.20	0.82	1.10	
	632	7.25	1.30	7.15	1.75	1.11	
	850	9.75	5.20	9.30	7.10	1.15	
	1,130	13.0	18.00	12.10	24.00	1.17	
	1,310	15.0	36.00	12.85	50.00	1.20	
24							

$$\tau_{cr} = 12.8 \times 10^5$$

$$\tau_{cr} \times M_w = 6.37 \times 10^{11}$$

Table I-7

Polystyrene

$$\bar{M}_w = 498,000$$

$$\bar{M}_w/\bar{M}_n = <1.20$$

Temperature: 230°C

L/D	ΔP (psi)	$\tau_{ap} \times 10^{-5}$ dynes/cm ²	$4Q/\pi r_o^3$ (sec ⁻¹)	$\tau_w \times 10^{-5}$ dynes/cm ²	$\dot{\gamma}_w$ (sec ⁻¹)	D_s/D	Remarks
10	415		4.00			1.02	
	543	9.35	11.00	8.90	14.70	1.09	
	606	10.40	15.80	9.70	21.00	1.12	
	724	12.40	29.00	11.10	39.00	1.15	
	815	14.0	42.50	11.70	57.50	1.19	
	1,020	17.50	104.	13.00	135.	1.22	Fracture
15	815	9.36	10.0	9.05	14.30	1.19	
	905	10.40	14.90	9.90	19.50	1.21	
	1,085	12.50	30.00	11.50	40.50	1.22	
	1,240	14.30	54.00	12.10	74.00	1.25	
	1,360	15.60	85.20	12.80	115.0	1.25	
	1,400	16.10	102.0	13.00	135.00	1.26	Fracture
24							

$$\tau_{cr} = 13.0 \times 10^5$$

$$\tau_{cr} \times M_w = 6.47 \times 10^{11}$$

Table I-8

Polystyrene

$$\bar{M}_w = 600,000$$

$$\bar{M}_w/\bar{M}_n = 2.32$$

Temperature: 200°C

L/D	ΔP (psi)	$\tau_{ap} \times 10^{-5}$ dynes/cm ²	$4Q/\pi r_0^3$ (sec ⁻¹)	$\tau_w \times 10^{-5}$ dynes/cm ²	$\dot{\gamma}_w$ (sec ⁻¹)	D_s/D	Remarks
10	690	11.85	20	8.30	26.00	1.68	Fracture
	836	14.40	27.4	9.05	36.80	1.82	
	928	16.00	33.5	9.52	45.90	1.95	
	980	16.40	38.0	9.80	52.00	1.96	
	1,150	19.80	56.0	10.75	77.00	2.24	
	1,270	21.80	72.0	11.40	100.00	2.30	
15	836	9.65	16.5	8.50	21.50	1.67	Fracture
	980	11.30	22.0	9.30	29.00	1.74	
	1,150	13.25	31.0	9.70	41.80	1.82	
	1,221	14.00	36.0	9.70	48.70	2.06	
	1,460	16.80	57.5	10.72	78.70	2.10	
	1,590	18.30	71.50	11.40	100.00	2.18	
19.5	1,130	10.00	22.0	8.50	29.00	1.96	Fracture
	1,335	11.80	28.50	9.20	38.20	2.04	
	1,460	12.90	34.50	9.55	47.00	2.10	
	1,590	14.00	43.00	10.10	58.70	2.15	
	1,830	16.20	65.50	11.12	90.00	2.20	
	1,890	16.70	71.80	11.40	100.00	2.21	

$$\tau_{cr} = 11.4 \times 10^5$$

$$\tau_{cr} \times M_w = 6.85 \times 10^{11}$$

Table I-9

Polystyrene

$$\bar{M}_w = 670,000$$

$$\bar{M}_w/\bar{M}_n = <1.20$$

Temperature: 250°C

L/D	ΔP (psi)	$\tau_{ap} \times 10^{-5}$ dynes/cm ²	$4Q/\pi r_0^3$ (sec ⁻¹)	$\tau_w \times 10^{-5}$ dynes/cm ²	$\dot{\gamma}_w$ (sec ⁻¹)	D_s/D	Remarks
10	430	7.40	9.4	5.10	12.80	1.02	Fracture
	596	10.30	19.50	6.00	42.00	1.12	
	680	11.70	27.50	6.34	52.00	1.16	
	814	14.00	46.0	6.95	84.00	1.19	
	975	16.80	86.0	7.96	160.00	1.90	
	1,010	17.40	95.0	8.20	180.00	1.90	
15	860	9.90	26.50	6.20	43.00	1.18	Fracture
	975	11.20	41.0	6.82	76.00	1.32	
	1,040	12.00	50.0	7.10	94.00	1.40	
	1,150	13.20	68.50	7.56	126.00	1.40	
	1,245	14.30	88.0	8.00	163.00	1.40	
	1,270	14.60	94.0	8.20	180.00	1.40	
24	602	4.33	4.40	3.50	5.10	1.06	Fracture
	705	5.08	5.50	4.05	7.20	1.10	
	975	7.02	14.0	4.90	21.0	1.15	
	1,110	8.00	21.0	6.00	42.00	1.20	
	1,450	10.45	55.0	7.21	100.00	1.27	
	1,700	12.20	93.0	8.20	180.000	1.40	

$$\tau_{cr} = 8.2 \times 10^5$$

$$\tau_{cr} \times M_w = 5.5 \times 10^{11}$$

Table I-10

Polystyrene

$$\bar{M}_w = 760,000$$

$$\bar{M}_w/\bar{M}_n = 2.60$$

Temperature: 200°C

L/D	ΔP (psi)	$\tau_{ap} \times 10^{-5}$ dynes/cm ²	$4Q/\pi r_o^3$ (sec ⁻¹)	$\tau_w \times 10^{-5}$ Dynes/cm ²	$\dot{\gamma}_w$ (sec ⁻¹)	D_s/D	Remarks
10	452	7.78	4.00	5.40	5.47	1.46	Fracture
	679	11.70	10.00	6.90	13.00	1.58	
	836	14.40	16.00	7.30	21.50	1.70	
	974	16.75	23.00	7.60	31.50	1.86	
	1,192	20.00	40.00	8.75	55.0	2.12	
	1,360	23.40	60.20	9.65	85.00	2.18	
15	679	7.76	6.00	5.40	8.20	1.54	Fracture
	733	8.50	7.15	6.00	10.00	1.66	
	980	11.20	13.80	6.80	18.70	1.76	
	1,242	14.25	25.40	7.80	33.20	1.94	
	1,460	16.70	39.80	8.70	55.0	2.04	
	1,680	19.30	59.50	9.70	85.0	2.12	
19.5	980	8.62	7.50	6.10	10.80	1.74	Fracture
	1,175	10.35	14.10	6.70	19.20	1.89	
	1,242	10.91	17.50	7.00	24.0	1.92	
	1,460	12.85	27.70	8.00	37.0	2.00	
	1,560	13.70	33.00	8.35	45.0	2.10	
	1,880	16.50	59.00	9.75	85.00	2.40	

$$\tau_{cr} = 9.7 \times 10^5$$

$$\tau_{cr} \times M_w = 7.36 \times 10^{11}$$

Table I-11

Polystyrene

$$\bar{M}_w = 1.06 \times 10^6$$

$$\bar{M}_w/\bar{M}_n = 2.31$$

Temperature: 200°C

L/D	ΔP (psi)	$\tau_{ap} \times 10^{-5}$ dynes/cm ²	$4Q/\pi r_o^3$ (sec ⁻¹)	$\tau_w \times 10^{-5}$ dynes/cm ²	$\dot{\gamma}_w$ (sec ⁻¹)	D_s/D	Remarks
10	557	9.60	3.30	7.30	4.10	1.29	Fracture
	750	12.90	5.28	8.42	7.30	1.48	
	841	14.50	6.70	9.15	9.20	1.50	
	930	16.0	8.50	9.85	11.50	1.51	
	987	17.0	10.10	10.20	14.0	1.54	
	1,080	18.6	13.50	10.55	19.00	1.72	
15	605	6.95	2.50	5.00	3.0	1.29	Fracture
	750	8.62	3.20	6.20	4.20	1.30	
	836	9.63	3.80	7.36	5.20	1.40	
	1,038	11.95	5.80	8.72	8.00	1.45	
	1,250	14.40	9.60	10.1	13.20	1.58	
	1,400	16.10	13.30	10.65	19.00	1.79	
24							

$$\tau_{cr} = 10.6 \times 10^5$$

$$\tau_{cr} \times M_w = 11.2 \times 10^{11}$$

Table I-12

Polystyrene

$$\bar{M}_w = 1.8 \times 10^6$$

$$\bar{M}_w/\bar{M}_n = < 1.20$$

Temperature: 230°C

L/D	ΔP (psi)	$\tau_{ap} \times 10^{-5}$ dynes/cm ²	$4Q/\pi r_0^3$ (sec ⁻¹)	$\tau_w \times 10^{-5}$ dynes/cm ²	$\dot{\gamma}_w$ (sec ⁻¹)	D_s/D	Remarks
10	360	6.20	0.50	4.35	0.63	1.10	Fracture
	430	7.40	0.72	4.96	0.95	1.15	
	496	8.53	1.00	5.50	1.30	1.18	
	540	9.30	1.22	5.73	1.65	1.24	
	650	11.20	1.96	6.30	2.70	1.35	
	710	12.20	2.50	6.80	3.60	1.40	
15	452	5.20	0.46	4.05	0.60	1.15	Fracture
	540	6.20	0.62	4.83	0.85	1.20	
	632	7.27	0.88	5.43	1.20	1.32	
	740	8.52	1.26	6.00	1.75	1.35	
	840	9.65	1.91	6.35	1.65	1.40	
	900	10.40	2.54	6.83	3.61	1.43	
24	800	5.75	0.6	4.87	0.83	1.12	Fracture
	900	6.50	0.86	5.34	1.18	1.17	
	1,040	7.50	1.30	5.91	1.79	1.24	
	1,150	8.30	1.84	6.25	2.54	1.30	
	1,221	8.80	2.30	6.62	3.45	1.37	
	1,250	9.00	2.47	6.79	3.60	1.40	

$$\tau_{cr} = 6.8 \times 10^5$$

$$\tau_{cr} \times M_w = 12.2 \times 10^{11}$$

Table I-13

Polystyrene

$$\bar{M}_w = 1.8 \times 10^6$$

$$\bar{M}_w/\bar{M}_n = < 1.20$$

Temperature: 250°C

L/D	ΔP (psi)	$\tau_{ap} \times 10^{-5}$ dynes/cm ²	$4Q/\eta r_0^3$ (sec ⁻¹)	$\tau_w \times 10^{-5}$ dynes/cm ²	$\dot{\gamma}_w$ (sec ⁻¹)	D_s/D	Remarks
10	340	5.85	2.18	4.55	3.00	1.05	Fracture
	496	5.55	3.80	5.72	5.20	1.19	
	588	10.10	5.20	6.10	7.30	1.20	
	680	11.70	7.20	6.66	10.00	1.25	
	700	12.00	7.75	6.867	10.50	1.25	
	730	12.60	8.70	7.15	12.80	1.25	
15	465	5.35	2.10	4.47	2.95	1.25	Fracture
	557	6.40	2.80	5.30	3.90	1.27	
	705	8.10	4.35	5.92	6.10	1.30	
	750	8.63	5.00	6.00	8.30	1.32	
	841	9.65	6.50	6.46	9.00	1.32	
	930	10.70	8.60	7.10	12.80	1.32	
24	605	4.33	1.3	3.70	1.75	1.07	Fracture
	836	6.02	2.6	5.32	3.50	1.12	
	1,080	7.78	5.0	6.07	8.30	1.19	
	1,192	8.60	6.6	6.53	9.20	1.24	
	1,245	9.00	7.4	6.80	10.80	1.26	
	1,330	9.60	8.80	7.25	12.80	1.26	

$$\tau_{cr} = 7.15 \times 10^5$$

$$\tau_{cr} \times M_w = 12.9 \times 10^{11}$$

APPENDIX II

At low shear rates according to White (35)

$$\tau_{zz} - \tau_{rr} = 2\tau_{zr}S_R \quad (\text{II-1})$$

Also at low shear rates

$$\tau_{zz} - \tau_{rr} = k_N \dot{\gamma}^2 \quad (\text{II-2})$$

Combine equations (II-1) and (II-2) and we obtain

$$2\tau_{zr}S_R = k_N \dot{\gamma}^2 \quad (\text{II-3})$$

But $\dot{\gamma} = \frac{\tau_{zr}}{\eta_0}$ for low shear rates. So equation (II-3) becomes

$$2\tau_{zr}S_R = k_N \frac{\tau_{zr}^2}{\eta_0^2}$$

or

$$S_R = k_N \frac{\tau_{zr}}{2\eta_0^2} \quad (\text{II-4})$$

But for a monodisperse collection of Rouse chains

$$k_N = k_R = \frac{2n^2}{15} \eta_0 \lambda_R = \frac{2\tau^2}{15} \eta_0 \frac{6}{\eta^2} \frac{\eta_0 \bar{M}_w}{\rho RT}$$

So

$$k_N = k_R = \frac{4}{5} \eta_0^2 \frac{\bar{M}_w}{\rho RT} \quad (\text{II-5})$$

Substituting equation (II-5) into (II-4) we obtain

$$S_R = \frac{4}{5} \eta_0^2 \frac{\bar{M}_w}{\rho_{RT}} \frac{\tau_{zr}}{2\eta_0^2} = \frac{2}{5} \frac{\bar{M}_w \tau_{zr}}{\rho_{RT}}$$

APPENDIX III

At low shear rates

$$\tau_{zz} - \tau_{rr} = k_N \dot{\gamma}^2 \quad (\text{III-1})$$

where k_N is the normal stress coefficient.

For a polydisperse collection of Rouse chains

$$k_R = \frac{2n^2}{15} \eta_0 \lambda_R \frac{\bar{M}_z \bar{M}_{z+1}}{\bar{M}_w^2} \quad (\text{III-2})$$

where

$$\lambda_R = \frac{6}{\eta^2} \frac{\eta_0 \bar{M}_w}{\rho RT} \quad (\text{III-3})$$

An experimental time constant associate with the normal stress can be evaluated as

$$\lambda_N = \frac{15k_N}{2\eta_0 n^2} \frac{\bar{M}_w^2}{\bar{M}_z \bar{M}_{z+1}} \quad (\text{III-4})$$

where

$$k_N = \frac{\tau_{zz} - \tau_{rr}}{\dot{\gamma}^2} \quad (\text{III-5})$$

(at low shear rates).

But, according to White (35),

$$\tau_{zz} - \tau_{rr} = 2S_R \times \tau_{zr} \quad (\text{III-6})$$

So equation (III-5) becomes

$$k_N = \frac{2S_R \times \tau_{zr}}{\dot{\gamma}^2} = 2J\eta_0^2 \quad (\text{III-7})$$

where

$$J = \frac{s_R}{\tau_{rz}}$$

Combining equations (III-7) and (III-4) we obtain

$$\lambda_N = \frac{15J\eta_0^2}{\eta_0\eta^2} \frac{\overline{M}_w^2}{\overline{M}_z\overline{M}_{z+1}} \quad (\text{III-8})$$

If we divide equations (III-8) and (III-3) we obtain

$$\frac{\lambda_N}{\lambda_R} = \frac{5}{2} \frac{\overline{M}_w^2}{\overline{M}_z\overline{M}_{z+1}} \frac{\rho_{RT}}{\overline{M}_w} J \quad (\text{III-9})$$

But for a polydisperse collection of Rouse molecules the steady-state shear compliance is (70)

$$J_R = \frac{2}{5} \frac{\overline{M}_z\overline{M}_{z+1}}{\overline{M}_w^2} \frac{\overline{M}_w}{\rho_{RT}}$$

So equation (III-9) becomes

$$\frac{\lambda_N}{\lambda_R} = \frac{J}{J_R}$$

for low shear rates.